

Accepted Manuscript

Design and discovery of silybin analogues as antiproliferative compounds using a ring disjunctive – Based, natural product lead optimization approach

Elangovan Manivannan, PhD, Haneen Amawi, Noor Hussein, Chandrabose Karthikeyan, Aubry Fetcenko, N.S. Hari Narayana Moorthy, Piyush Trivedi, Amit K. Tiwari, PhD

PII: S0223-5234(17)30191-5

DOI: [10.1016/j.ejmech.2017.03.033](https://doi.org/10.1016/j.ejmech.2017.03.033)

Reference: EJMECH 9293

To appear in: *European Journal of Medicinal Chemistry*

Received Date: 29 December 2016

Revised Date: 10 February 2017

Accepted Date: 15 March 2017

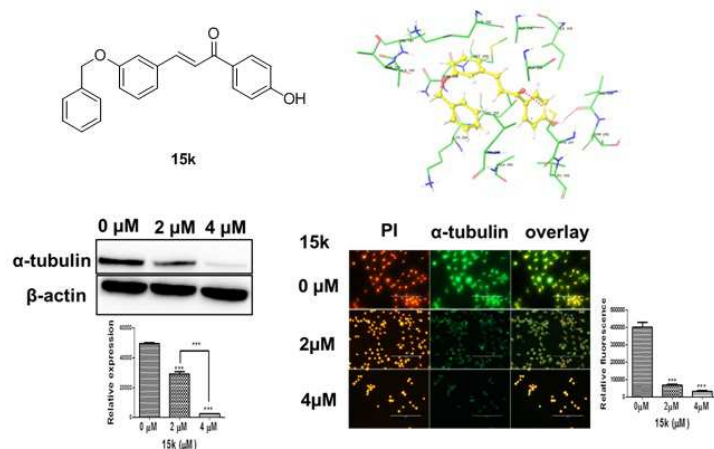
Please cite this article as: E. Manivannan, H. Amawi, N. Hussein, C. Karthikeyan, A. Fetcenko, N.S.H. Narayana Moorthy, P. Trivedi, A.K. Tiwari, Design and discovery of silybin analogues as antiproliferative compounds using a ring disjunctive – Based, natural product lead optimization approach, *European Journal of Medicinal Chemistry* (2017), doi: 10.1016/j.ejmech.2017.03.033.

This is a PDF file of an unedited manuscript that has been accepted for publication. As a service to our customers we are providing this early version of the manuscript. The manuscript will undergo copyediting, typesetting, and review of the resulting proof before it is published in its final form. Please note that during the production process errors may be discovered which could affect the content, and all legal disclaimers that apply to the journal pertain.



Graphical Abstract

Described herein is design and synthesis of novel silybin derivatives using natural lead optimization and ring disjunctive approach leading to discovery of a lead compound **15k**, which produces apoptosis in ovarian cancer cells through tubulin inhibition



Design and discovery of silybin analogs as antiproliferative compounds using a ring disjunctive – based, natural product lead optimization approach

Elangovan Manivannan^{a,*}, Haneen Amawi^{b,#}, Noor Hussein^b, Chandrabose Karthikeyan^c, Aubry Fetcenko^b, N.S. Hari Narayana Moorthy^c, Piyush Trivedi^c, Amit K. Tiwari^{b,*}

^a*School of Pharmacy, Devi Ahilya Vishwavidyalaya, Indore, (MP) 452001, India*

^b*Department of Pharmacology and Experimental Therapeutics, College of Pharmacy & Pharmaceutical Sciences, University of Toledo, OH, USA*

^c*School of Pharmaceutical Sciences, Rajiv Gandhi Proudhyogiki Vishwavidyalaya, Airport Bypass Road, Gandhi Nagar, Bhopal (MP) 462036, India*

Running title: *Novel silybin analogs display potent tubulin inhibition*

Note: First two authors contributed equally to this work.

***Corresponding Authors:**

Amit K. Tiwari, PhD

Department of Pharmacology and Experimental Therapeutics,
College of Pharmacy & Pharmaceutical Sciences,
University of Toledo, Ohio 43614

Tel: 419-383-1913

Fax: 419-383-1909

E-mail: amit.tiwari@utoledo.edu

Elangovan Manivannan, PhD

Medicinal & Pharmaceutical Chemistry,
School of Pharmacy, Devi Ahilya Vishwavidyalaya,
Indore, M.P., India 452001

Tel: +91-7509114754

E-mail: drmanislab@gmail.com

Abstract

The present study reports the synthesis and anticancer activity evaluation of twelve novel silybin analogues designed using a ring disjunctive-based natural product lead (RDNPL) optimization approach. All twelve compounds were tested against a panel of cancer cells (i.e. breast, prostate, pancreatic, and ovarian) and compared with normal cells. While all of the compounds had significantly greater efficacy than silybin, derivative **15k** was found to be highly potent ($IC_{50} < 1 \mu M$) and selective against ovarian cancer cell lines, as well as other cancer cell lines, compared to normal cells. Preliminary mechanistic studies indicated that the antiproliferative efficacy of **15k** was mediated by its induction of apoptosis, loss of mitochondrial membrane potential and cell cycle arrest at the sub-G1 phase. Furthermore, **15k** inhibited cellular microtubules dynamic and assembly by binding to tubulin and inhibiting its expression and function. Overall, the results of the study establish **15k** as a novel tubulin inhibitor with significant activity against ovarian cancer cells.

Keywords: Silybin, ring disjunctive natural product lead optimization, (E)-3-(3-(benzyloxy)phenyl)-1-phenylprop-2-en-1-one, tubulin inhibitor, chemoprevention

Introduction

Natural products research has helped elucidate previously unknown biochemical mechanisms, while identifying several clinically effective anticancer drugs, such as paclitaxel, doxorubicin, vinblastine, and vincristine [1]. Silymarin is a polyphenolic flavonoid complex found in the dried fruits of the milk thistle plant (*Silybum marianum*) [2-4]. Over the last few decades, the pharmacological properties of different components of silymarin i.e. silybin A (**1**), silybin B (**2**), isosilybin A (**3**), isosilybin B (**4**), silychristin (**5**), isosilychristin (**6**), silydianin (**7**) and (+)-taxifoline (**8**) as shown in (**Figure 1**) have been extensively investigated [5-13]. Of these aforementioned compounds, silybin was found to be the most potent antiproliferative component of silymarin and it has been reported to inhibit numerous cancers, including breast [14, 15], colon [16], liver [17, 18], lung [19], ovary [20], prostate [21-23], and skin cancer [24, 25]. Silybin's cytotoxic and chemopreventive efficacy results from concomitantly targeting multiple important cancer targets [17]. For example, silybin 1) produces cell cycle arrest at both the G1/ and G2 phase;s 2) activates Erb1 signalling; 3) induces cyclin-dependent kinase (CDK) inhibition; 4)down-regulates specific anti-apoptotic proteins; , 5) inhibits kinases required for cell survival and 6) inhibits inflammatory transcription factors [21, 24, 26-31]. Furthermore, silybin produces antimetastatic activity by targeting dysregulated stemness pathways, such as the Wnt/beta-catenin/epithelial to mesenchymal transition (EMT). Both *in vitro* and *in vivo* studies indicate that silybin has an excellent safety profile, with no significant induction of toxicity or carcinogenesis at doses up to 1200 mg daily [32]. Although silybin, a polyphenolic natural product, has anticancer efficacy in preclinical models, its pharmacokinetic limitations such as poor absorption, rapid metabolism, and poor bioavailability has hampered its clinical use [33].

Attempts to overcome these issues with structural modifications of the phenol and alcohol functions of silybin [5, 34] through esterification [35], phosphorylation [36], glycosidation [33], and oxidation of the C-23 alcohol [37] have had limited success.

Structural modification of a natural product lead (NPL) is a frequently used approach in NPL based drug discovery. NPL optimization can be used to attain novel bioactive molecules with improved pharmacological and PK properties, along with target selectivity [38, 39]. The strategy of splitting fused ring structures of NPL by following a 'disjunctive approach', more often results in new bioactive molecules with a similar mechanism of action and improved PD/PK [40, 41]. Herein, we report a NPL optimization strategy consisting of sequential exclusion of functional groups, and a ring disjunctive approach coupled with exploration of different functional groups on the silybin core structure. Simplification of the silybin core structure by removing functionality, chirality and ring opening, allowed us to identify the minimum pharmacophore required for efficacy to inhibit cancer cell proliferation. This strategy also resulted in the identification of an anticancer lead, (E)-3-(3-(benzyloxy) phenyl)-1-phenylprop-2-en-1-one (**15a**). We further optimized **15a** by substituting advantageous functional groups to obtain more potent derivatives. The design, synthesis, identification, SAR, and antiproliferative profile of these derivatives are reported herein. In addition, additional pharmacodynamic mechanisms (cytotoxicity, anti-apoptosis and tubulin inhibition) of the optimized molecule **15k** are identified and reported herein.

2. Results & Discussion

2.1 Chemistry of new silybin analogues

General methods for the preparation of chalcones involve the Claisen–Schmidt condensation of appropriate aryl methyl ketones and aldehydes in the presence of either an acid or base [42]. The compounds, **15a** – **15k**, were prepared by reacting 3-(benzyloxy) benzaldehyde (**12**) with the appropriate acetophenones (**14a** – **14k**), in presence of dilute potassium hydroxide at room temperature (**Scheme 1**). Similar reaction conditions were used for the synthesis of unsubstituted chalcone, (**17**) using unsubstituted benzaldehyde (**Scheme 2**). Furthermore, all reactions resulted in the formation of chalcone derivatives **15a** – **15k** and **17** in good yield as shown in **Figure 2**. The structures of all the compounds were established by the use of IR, ¹H-NMR, and mass spectral data. The elemental analysis of the final compounds was found to be within ± 0.3 % limit. The physico-chemical and spectral data of all the final compounds **15a** – **15k** have been furnished in materials and method section. In the IR spectra, the absorption bands due to stretching frequency of olefinic double bonds appeared between 1603 to 1592 cm⁻¹ whereas the absorption bands due to aromatic stretch appeared at 1600.8 and 1506.3 cm⁻¹. The absorption bands due to carbonyl stretch (C=O) appeared between 1679 to 1650 cm⁻¹. The absorption bands due bending vibrations of aliphatic and aromatic C–H appeared at 1467.7 and 827.4 cm⁻¹, respectively, in the spectrum which confirms the formation of all synthesized compounds. ¹H NMR spectra showed that typically *E*-isomers were generated in this reaction. In the ¹H NMR spectra of chalcones (**15a** – **15k**), the protons of α, β-unsaturated system absorbed as two doublets around δ 7.4 ppm for H_a and δ 7.9 for H_b with coupling constant *J* = 15–16 Hz. The aromatic hydrogens appear at δ 6.5–8.5 ppm

depending on the substituent on the aromatic (Ar) group. The singlet signals at the region between δ 7.5 and 8.5 ppm are attributed to the resonance of the 1,4-phenylene ring hydrogens. A singlet for two protons of Ph-(CH₂)-O- appeared downfield at δ 5.12. Furthermore the mass spectrum of all the synthesized compounds (**15a** – **15k**) showed the molecular ion peak i.e. m/z (M+1), which confirmed their synthesis. The functional group transformation of -CHO into -CO-CH=CH- in compounds (**15a** – **15k**) was established on the basis of IR, ¹H NMR and mass spectral data.

2.2 Natural product lead optimization of silybin

Silybin's antiproliferative efficacy (IC₅₀~80-222 μ M) has been previously validated in multiple studies [43-46]. In the present study, we selected silybin as a cytotoxic lead for medicinal chemistry optimization. First, we characterized the detailed role of ring structures and the respective hydroxyl groups of silybin. This helped guide the systematic structural modification and lead optimization of silybin to obtain a more potent proliferation inhibitor with specificity for neoplastic cells. Silybin is nearly a 1:1 mixture of two diastereomers, namely silybin A (**1**) and silybin B (**2**). Structurally, the isomers of silybin represent a typical flavonolignan scaffold. Silybin A (**1**) is characterized by five ring structures, with alternating carbo- and heterocycles (ring A to ring E) and five hydroxyl groups. The five hydroxyl groups of silybin A (**1**) are the main targets for derivatization [5]. These hydroxyl groups can be divided into three categories according to their nature: three phenolic (two in A and one in E ring), one secondary (in B Ring) and one primary alcoholic group (in D ring). For example, we considered the antiproliferative efficacy of silybin and its analogues (**9** and **10**) in the breast cancer cell

line, MCF-7, as previously reported by Zhao H et. al., to describe our disjunctive approach based on a natural product lead optimization strategy [34]. Silybin inhibited MCF-7 cell proliferation ($IC_{50} = 222.8 \pm 3.6 \mu\text{M}$). The modification steps are described in details in **Figure 2**. In brief, we first removed the two phenolic substituents of ring A in silybin A **1**, resulting in analogue **9** that was approximately 16-fold more potent than silybin, with an IC_{50} value of $13.8 \pm 3.6 \mu\text{M}$ in MCF-7 cells. The increase in efficacy may be due to an increase in solubility. In the second step, we used a disjunctive approach to open ring B of the silybin analogue **9**, followed by removal of a hydroxyl group and introduction of a double bond. The resulting silybin analogue **10**, was only slightly more potent (IC_{50} value of $12 \pm 0.2 \mu\text{M}$) than silybin in MCF-7 cells. In the third step, we cleaved ring D and removed all hydroxyl and a methoxy groups to derive a new silybin analogue, **15a**, whose IC_{50} value ($9.8 \pm 3.0 \mu\text{M}$) in MCF-7 cells was lower than that for analogues 9 and 10. It should also be noted that **15a** had differential inhibitory efficacy on breast cancer proliferation in other breast cancer cell lines, i.e. ZR-75-1 ($IC_{50} = 8.4 \pm 0.9 \mu\text{M}$), BT-20 ($IC_{50} = 25.5 \pm 0.2 \mu\text{M}$), and MDAMB-231 ($IC_{50} = 19.7 \pm 1.9 \mu\text{M}$). In the fourth step, we cleaved ring E to derive a compound, **17**, with an IC_{50} value of $12.6 \pm 6 \mu\text{M}$ in MCF-7 cells.

We ended our disjunctive approach at the third step and kept the 3-(3-(benzyloxy)phenyl)-1-phenylprop-2-en-1-one backbone (**15a**) and systematically varied the substituents of ring A of **15a** with respect to the hydroxyl positions of silybin A (**1**). This resulted in synthesis of compounds **15b – 15k**, with some of these compounds having electron withdrawing groups (EWG), such as 2-chloro, 2,4-dichloro, 2,3,4-trichloro, 2-bromo, 3-bromo, 4-bromo and 4-nitro, followed by some electron donating

groups (EDG) (4-methoxy 4-methyl and 4-hydroxy). The introduction of a 2-bromo substitution on ring A of 3-(3-(benzyloxy)phenyl)-1-phenylprop-2-en-1-one **15h** ($IC_{50} = 1.6 \pm 0.9 \mu\text{M}$) on MCF-7 resulted in a ≈ 140 -fold increase in cytotoxic activity compared to silybin.

2.3 Antiproliferative efficacy and the structure-activity relationships for the novel silybin analogues

In the process of optimizing the NPL silybin A (**1**) and designing novel analogues, we prepared and evaluated a series of (E)-3-(3-(benzyloxy)phenyl)-1-phenylprop-2-en-1-one analogues to determine their antiproliferative efficacy in eleven different cell lines: three normal cell lines (normal epithelial colon cells: CRL-1459, human embryonic kidney cells: HEK293/pcDNA.3.1, and Chinese hamster ovarian cells: CHO) and eight cancer cell lines [human breast adenocarcinoma (MCF-7), human metastatic breast cancer (ZR-75-1), human breast carcinoma (BT-20), human breast adenocarcinoma (MDAMB-231), human prostate adenocarcinoma (DU-145), human pancreatic adenocarcinoma (PANC1), human ovarian carcinoma (OV2008) and human ovarian carcinoma (A2780) cells] using the MTT assay. The antiproliferative efficacy data are presented as the IC_{50} values, defined as the concentration of compound that decreases cell proliferation by 50% (**Table 1**). The IC_{50} values were generated from at least three independent experiments.

Compounds **15a** – **15f** had IC_{50} values ranging from ~ 5 to $81 \mu\text{M}$ for different cancer cells. The unsubstituted benzyloxy derivative **15a** exhibited significant antiproliferative

efficacy. Compound **15a** was efficacious in inhibiting the proliferation of MCF-7, ZR-75-1, BT-20, MDAMB-231, DU-145, PANC1, OV2008 and A2780 cancer cell lines, with IC_{50} values of 9.8 ± 3.0 , 8.6 ± 0.9 , 25.5 ± 0.2 , 20.0 ± 1.9 , 42.4 ± 7.1 , 23.5 ± 1.7 , 4.9 ± 1.4 , and $6.7 \pm 0.7 \mu\text{M}$, respectively. Additionally, the first set of synthesized compounds (**15a – 15f**) exhibited moderate to good antiproliferative efficacy against all the cancer cell lines tested. Also, it should be noted that the potency of most of the compounds was generally greater for the cancer cells compared to the normal cell lines CRL-1459, HEK293/pcDNA.3.1 and CHO.

The chalcone derivative **17** (without benzyloxy moiety) showed moderate antiproliferative efficacy for the breast cancer lines MCF-7 ($IC_{50} = 12.6 \pm 1.5 \mu\text{M}$), ZR-75-1 ($IC_{50} = 13.7 \pm 0.9 \mu\text{M}$), BT-20 ($IC_{50} = 21.1 \pm 0.9 \mu\text{M}$), and MDAMB-231, ($IC_{50} = 6.7 \pm 0.9 \mu\text{M}$) It showed significantly lower inhibition for DU-145, PANC1 and OV2008, A2780 cancer cells, with IC_{50} values of 52.5 ± 3.1 , 23.5 ± 1.7 , 33.4 ± 2.1 , and 67.4 ± 4.3 respectively. However, its counterpart benzyloxy derivative **15a**, exhibited better antiproliferative efficacy in both ovarian cancer cell lines OV2008 ($IC_{50} = 4.9 \pm 1.4 \mu\text{M}$) and A2780 ($IC_{50} = 6.7 \pm 0.7 \mu\text{M}$). The structure–activity relationship (SAR) analysis suggested that the 3-benzyloxy moiety enhanced the antiproliferative efficacy, particularly in ovarian cancer cell lines. Therefore, it can be concluded that the benzyloxy group (ring E) attached to 3-position of chalcone (ring D) is crucial for increasing antiproliferative activity against breast and ovarian cancers. The present SAR is in good agreement with the previously published reports indicating that the benzyloxy group augments the antiproliferative or cytotoxic efficacy [47, 48].

Interestingly, we found that altering the substituents at the 2- and 4-positions of ring A (phenyl) of the silybin analogues could also significantly affect the antiproliferative efficacy. By introducing EWGs on ring A, three compounds (**15b**, **15c**, and **15d**) were generated that possessed improved efficacy compared to chalcone (**17**), except for breast cancer cell lines. In fact, compounds **15b** and **15c** with EWGs displayed an enhanced potency in comparison to that of **15d**, whereas compounds **15e** and **15f** with EDGs showed a decreased antiproliferative efficacy against all the cancer cell lines. However, compound **15d**, with a nitro substitution at the 4th position, was less efficacious than the chloro substituted compounds **15b** and **15c** (**Table 4**). Similarly, compound **15f**, which has a polar 4-methoxy substituent, was also lower antiproliferative efficacy. However, the remaining compounds had significantly increased potencies, suggesting that a concurrent increase in electronegativity and hydrophobicity of the compounds increased the efficacy.

When the 4th position of ring A was substituted with small alkyl groups (methyl), the efficacy was not significantly increased. Compound **15e**, with a methyl substitution on ring A, was moderately efficacious in inhibiting proliferation of MCF-7, ZR-75-1, BT-20, MDAMB-231, DU-145, PANC1, OV 2008 and A2780 cancer cell lines, with IC₅₀ values of 21.7 ± 1.1, 25.8 ± 4.2, 61.0 ± 3.5, 15.6 ± 2.3, 25.6 ± 3.5, 41.6 ± 1.6, 12.9 ± 0.9 and 20.1 ± 1.9 μM, respectively. However, it was more cytotoxic against HEK293/pcDNA.3.1 cells, with an IC₅₀ value of 8.2 ± 0.3. Interestingly, the alkoxy derivative **15f** was more active on the breast cancer cell lines MCF-7, ZR-75-1, BT-20, MDAMB-231 and with IC₅₀ values of 6.0 ± 0.9, 19.9 ± 0.9, 38.3 ± 5.1, 12.4 ± 1.4 μM, respectively, than the alkyl derivative, **15e**, suggesting that the electronic influence of ring A significantly

affects the breast cancer efficacy. Collectively, our result clearly indicate that the hydrophobicity on ring A at the 2,4-position of the synthesized newer silybin analogs is beneficial to their antiproliferative efficacy. It should be noted that most of the compounds tested in this study were less toxic to normal cells compared to cancer cells, suggesting that the silybin analogues were selectively toxic to cancer cells compared to the non-malignant, normal cells. Furthermore, compounds **15a–15f** displayed poor antiproliferative efficacy for both prostate (DU-145) and pancreatic (PANC1) cancer cell lines compared to their efficacy to inhibit breast cancer cells growth. Based on the above results, the SAR were not immediately apparent because of the limited number of compounds tested and the positions for the substituents yielded differential antiproliferative efficacies. Owing to antiproliferative efficacy of **15a** and **15f**, they were subjected to further medicinal chemistry optimization and SAR investigations to develop more potent, selective and broad spectrum anticancer compounds. A set of four compounds bearing EWGs, i.e. 2,3,4-trichloro **15g**, 2-bromo **15h**, 3-bromo **15i**, 4-bromo **15j** and a compound bearing an EDG 4-hydroxy, **15k**, were synthesized and assessed for their efficacy to inhibit tumor cell growth. As anticipated from the previous SAR experiments, the newly synthesized compounds **15g–15k**, had significant antiproliferative efficacy (ranging from 0.3 – 9 μM) in all of the tested cancer cell lines (except **15h** for PANC1, with an IC_{50} = 61.2 μM).

The introduction of the chloro, bromo and hydroxyl groups at positions 2, 3, 4 of the ring A of the lead compound **15a** resulted in a significant improvement in antiproliferative efficacy (compare **15a–15f** with **15g–15k**). Compound **15g**, having 2,3,4-trichloro substitutions, had significant antiproliferative efficacy in all the breast cancer cell lines

compare to dichloro (**15c**) and mono chloro (**15b**) substituted compounds. We observed that when the number of chlorine atom increases in ring A of **15a**, the anti-cancer efficacy was found to also increase. Similarly, a significant increase in antiproliferative efficacy was observed for prostate cancer (DU-145; $IC_{50} = 6.4 \pm 0.5$) and pancreatic cancer cells (PANC1; $IC_{50} = 2.4 \pm 0.4$). In pancreatic cancer cell, the most potent compounds were **15g** and **15j**, with IC_{50} values 10-fold greater than the lead compound, **15a**. In particular, in this subset (**15g** – **15k**), the 2-bromo derivative, **15h**, had significant efficacy in MCF-7, ZR-75-1, BT-20, and MDAMB-231, breast cancer cell lines, with IC_{50} values of 1.6 ± 0.9 , 2.9 ± 0.1 , 1.8 ± 0.9 , and 1.9 ± 0.4 μ M, respectively. The 4-bromo derivative, **15j**, displayed a higher antiproliferative efficacy against all type of cancers. Its *meta* counterpart, the 3-bromo compound, **15i**, had low efficacy within this subset (**15g** – **15k**), indicating that a *meta* substitution on ring A of the lead **15a** minimizes antiproliferative efficacy. A bromo substitution was well tolerated on the 2 and 4 positions of ring A, was bromo substitution was not at the 3-position (compare **15h**, **15i**, **15j**). Compound **15h**, had IC_{50} values up to 6-fold higher than **15a** and 142 fold higher than silybin in MCF-7 cells. Overall, the replacement of a chlorine with bromine led to the 2-bromo **15h**, 3-bromo **15i**, and 4-bromo **15j** derivatives, which were more potent in all types of cancer cell lines ($IC_{50} \sim 1$ to 9 μ M) (except **15h** for PANC1, with an $IC_{50} \sim 61$ μ M), indicating that the larger bromine is preferred over chlorine. The exchange of the EWG group for a hydrophilic hydroxyl substituent in the 4-position, i.e. **15k**, was found to be beneficial for antiproliferative efficacy in MCF-7, ZR-75-1, BT-20, and MDAMB-231 breast cancer cell lines with IC_{50} values of 2.8 ± 0.9 , 4.9 ± 0.2 , 5.1 ± 2.1 , and 2.7 ± 0.6 μ M, respectively. In general, our results indicated that derivatives

carrying the EWGs at the 2nd and 4th positions on ring A of lead **15a** were typically the most efficacious against all of the cancer cell lines. .

2.4 The 15k has significant efficacy and selectively in inhibiting the growth of ovarian cancer cell lines.

With regard to the antiproliferative efficacy on ovarian cancer cells, compound **15a** had an IC₅₀ value of 4.9 ± 1.4 μM for OV2008 cells and an IC₅₀ value of 6.7 ± 0.7 μM for A2780 cells. Specifically, compound **15b**, with a 4-chloro substitution, has weak antiproliferative efficacy in both ovarian cell lines (OV2008; IC₅₀ = 20.0 ± 2.3 μM, A2780; IC₅₀ = 56.41 ± 2.78 μM). However, the 3,4- dichloro derivative, **15c**, was almost equipotent in OV2008 cells (IC₅₀ = 5.2 ± 1.1 μM), but less efficacious for A2780 (IC₅₀ = 21.4 ± 3.2 μM), compared to compound **15a**. The presence of three chlorine groups on the A-ring at the 2, 3, 4 position led to compound **15g** (OV2008; IC₅₀ = 1.5 ± 0.9 μM and A2780; IC₅₀ = 1.52 ± 0.02 μM), which had cytotoxic efficacy, but did not show any selectivity for normal cell lines. The insertion of a 4-nitro group on phenyl ring A led to derivative **15d**, that had low efficacy (up to 50 μM) toward both ovarian cell lines, whereas with an alkyl moiety (compound **15e**), the cytotoxic efficacy in the these cell lines was retained, although its efficacy is somewhat lower (OV2008; IC₅₀ = 12.85 ± 0.93 μM and A2780; IC₅₀ = 20.45 ± 1.90 μM) compared to compound **15c**. In comparison to compounds **15b**, **15c** (chloro substitution) **15h**, **15i**, and **15j** (bromo substitution) had greater efficacy in inhibiting ovarian cancer cell growth, The 2-bromo derivative, **15h**, was almost equipotent in both ovarian cancer cell lines (OV2008; IC₅₀ = 1.16 ± 0.42 μM and A2780; IC₅₀ = 2.48 ± 0.03 μM), compared to the 4-bromo derivative compound, **15j**, but had similar cytotoxicity towards normal cell lines (CRL-1459; IC₅₀ =

2.4 ± 0.9 µM and HEK293; IC₅₀ = 2.2 ± 0.0 µM). However, the 3-bromo derivative compound, **15i**, was less efficacious in ovarian cancer cell lines. The ortho and para isomers were 5-fold more efficacious than the meta isomer. Further, compounds without a benzyloxy substituent on ring E (compound **17**) were significantly less cytotoxic in ovarian cancer cells.

The antiproliferative efficacy data (**Table 3**) clearly indicates the significance of the hydroxyl derivative, **15k**, which was almost 6-fold more efficacious in OV2008 and A2780 cells (OV2008; IC₅₀ = 0.83 ± 0.1 µM and A2780; IC₅₀ = 0.97 ± 0.1 µM) compared to compound **15a**. Compound **15k** had a 9-10 fold greater IC₅₀ value for normal cell lines compared to ovarian cancer cell lines (**Figure 3A-3B**). The 4-position substituent of ring A considerably affected the inhibitory efficacy in ovarian cancer cells, with the hydroxyl and bromo substituents being the most favorable structural feature. The inhibition of ovarian cancer cells growth is encouraging as few compounds (especially compound **15k**) have achieved both sub micromolar potency and selectivity. Hence, compound **15k** was chosen for mechanism - based experiments on to determine how it inhibits ovarian cancer cell growth.

Following the incubation of ovarian cancer cells with different concentrations (0, 1, 2, or 4 µM), **15k** produced significant morphological changes in all the cells (see **Figure 3A** for representative images). We also determined if compound **15k** produced a time-dependent inhibition of ovarian cancer cell growth. Ovarian cancer cells were incubated with different concentrations of **15k** (0, 1, 2, 4, and 8 µM) and pictures were taken every two hours using the IncuCyte ZOOM® System (Biocompare, San Francisco, CA, USA) for 48h. The proliferation of ovarian cancer cells and confluence over time are

presented and quantified in Figures **3C** and **3D**. These data indicated that the antiproliferative efficacy of **15k** occurs within 12h and continues to inhibit the growth and proliferation of these cells over time (**Figures 3E and 3F**).

2.5 The 15k strongly induces apoptosis and induces sub-G1 cell cycle arrest in ovarian cancer cell lines

The induction of apoptosis, a form of programmed cell death, that produces (cell death, is one of the most important mechanisms by which several anticancer drugs exert their therapeutic effects [49]. The apoptogenic potential of a compound can be determined by its efficacy to produce a loss of the mitochondrial membrane potential, resulting in the release of several apoptogenic factors, including cytochrome c, among other mediators, in the apoptosis signalling pathway [49]. For example, during apoptosis, phosphatidylserine (PS) typically flips over to the extracellular side from its otherwise normal, intracellular mitochondrial localization [50]. The exposed PS readily binds to the fluorophore labelled human vascular anticoagulant protein (annexin V), with significant affinity, indicating the magnitude of apoptosis induction [51]. Compound **15k** produced significant apoptosis in both the OV2008 and A2780 ovarian cancer cell lines (**Figure 4**). In OV2008 cells, incubation treatment with **15k** for 12 h produced a loss of mitochondrial membrane potential (**Figure 4A**) and increased the population of cells undergoing apoptosis compared to control from 20% to 38% and 43% at 2 μ M and 4 μ M, respectively, (p value <0.001; **Figure 4B**). Similarly, the incubation of A2780 cells with **15 k** only up to 12 h produced significant apoptosis and a loss of the mitochondrial membrane potential (p value <0.001, **Figure 4A**). As shown in **Figure 4B**, 2 and 4 μ M of **15k**, respectively, produced a significant shift in the percentage of apoptosed cells

(37% and 38%, respectively) in quadrant II compared to 0% in the control group. Collectively, these results confirm the ability of this silybin derivative to reduce the mitochondrial membrane potential and induce apoptotic cell death.

To further assess the efficacy of compound **15k** to inhibit ovarian cancer cells proliferation, cell cycle analysis was conducted. The flow cytometry results indicated that compound **15k** increases the percentage of cells in sub G1 phase in a concentration - dependent manner (**Figure 4C and 4D**). The percentage of cells in the sub G1 phase increased from 11.3% control cells, to 25.5% and 34% with 2 and 4 μM of **15k**, respectively (p value <0.01 and 0.001, respectively). Additionally, **15k** significantly (p <0.001) decreased the percentage of cells in the G1 phase from 79% in the control cells to 58% and 45% after incubation with 2 and 4 μM , respectively, of **15k** (**Figures 4C and 4D**). However, **15k** at both concentrations (2 and 4 μM) did not significantly affect the percentage of cells in the S or G2 phases (**Figures 4C and 4D**). Thus, the antiproliferative efficacy of **15k** on ovarian cancer cells results, in part, from inducing cell cycle arrest at the sub-G1 phase.

2.6 **15k** inhibits α - tubulin expression in ovarian cancer cells

Tubulin is a major cellular protein and an essential component of the cellular cytoskeleton that polymerizes to form microtubules [4]. These microtubules are essential for cellular division, mitosis, intracellular transport, cell shape and polarity [52]. Both α - and β -tubulin polymerize into microtubules to form the mitotic spindle [53]. Accordingly, cell division takes place when these spindles move the chromosomes to the polar side of the cell [54]. Thus, alterations in the structure and/or function of microtubules can affect cell proliferation and survival [5]. Carcinogenesis has been

reported to be correlated with an increase in the polymerization and de-polymerization of tubulin [8]. Furthermore, a number of anticancer drugs have been developed to target and disrupt microtubular dynamics and prevent mitotic spindle formation, thereby inhibiting cell division and inducing cell cycle arrest and apoptosis [55]. Our silybin derivatives have a chalcone moiety in their structure which is known for tubulin inhibition and anticancer efficacy [56]. Thus, we determined the effect of **15k** on α - tubulin dynamic.

When **15k** was incubated overnight with OV2008 cancer cells at different concentrations (0, 2 μ M and 4 μ M), α -tubulin expression was significantly decreased ($p < 0.001$ for both concentrations) compared to control OV2008 cancer cells (**Figure 5A**). Also, using immunofluorescence, we validated the efficacy of **15k** on microtubule dynamics in ovarian OV2008 cancer cells. As shown in **Figure 5B**, in the control OV2008 cancer cells, there was a significant magnitude of green fluorescence, indicative of well – organized, spindle like microtubules arrayed along the long axes in the cytoplasm around the nucleus. In contrast, incubation of OV2008 cancer cells with **15k** (2 and 4 μ M) produced a significant disturbance in cellular microtubule shape and integrity. For example, the cells shrunk and became rounded and the microtubules no longer had a long spindle shape. Additionally, **15k**, at 2 and 4 μ M, induced a significant reduction ($p < 0.001$) in α - tubulin fluorescence intensity compared to control cells.

Molecular docking studies were performed in order to determine if **15k** was binding with α -tubulin. The colchicine binding pocket of tubulin (PDB ID: 1SA0, 3.58 Å) was used as a binding site for docking calculations as several chalcones that inhibit the assembly of tubulin are known to bind to this site [55, 57]. The ligands were docked into the

colchicine binding site of α -tubulin using Glide (Grid-Based Ligand Docking with Energetics) program of the Schrödinger molecular modeling suite (Schrödinger, Inc., New York, NY, 2012) [58]. Colchicine and **15k** were used for docking (**Figure 5C**). Initially, the docking protocol was validated through redocking DAMA-colchicine extracted from the X-ray structure to give a docked conformation very similar to the observed X-ray crystallographic conformation (root mean square deviation (rmsd) <0.69). Subsequently, the conformational library of compound **15k** was docked at the colchicine binding site of tubulin and the best fit conformation was selected on the basis of Glide score and visual inspection. **Figure 5D** shows the docked conformation of **15k** in the colchicine-binding site of tubulin. In this pose, the chalcone moiety aligns planar to the ring A and C of colchicine in the colchicine-binding site of tubulin **Figure 5E**. The phenyl ring B of chalcone overlaps ring A of colchicine, forming hydrophobic contacts with Lys352 β , Val181 α , Asn258 β , Met259 β and Ala316 β , whereas the phenyl ring A of the chalcone moiety is stabilized in the binding cavity through hydrophobic interactions with Ile378 β , Val238 β , Thr239 β , Leu242 β , Ala250 β and Leu255 β . Furthermore, the carbonyl oxygen of the enone group in chalcone moiety forms a hydrogen bond with the sulfhydryl group of Cys241 β . This is significant because colchicine shows a similar interaction with the tubulin[59]. Another hydrogen bond was also observed between the phenolic 'OH' in the para position phenyl ring B and nitrogen of Leu255 β . These two hydrogen bonds play a crucial role in stabilizing the orientation of chalcone moiety of **15k** in the colchicine-binding site. The unsaturated intermediate chain between rings A and B of chalcone moiety is also positioned in the vicinity of the side-chain of Ala316 β and Leu255 β . The phenyl ring C of **15k** forms a 'cis' like configuration relative to ring B of the chalcone moiety, establishing hydrophobic contacts with Ala250 β , Lys254 β and

Leu255 β . Collectively, Western blot analysis (**Figure 5A**), immunofluorescence (**Figure 5B**) and molecular docking analysis (**Figure 5C-E**) indicate that **15k** interacts with tubulin with high affinity and that it might exert its anticancer activity through lowering the expression and function of α -tubulin thus producing inhibition of microtubule assembly and cellular mitosis in the tested ovarian cancer cell lines. Thus, α -tubulin could be a major target for novel silybin derivative **15k**.

3. Conclusion

Here we report the design and synthesis of twelve novel derivatives of silybin using ring disjunctive based natural product lead optimization approach. All the compounds synthesized were found to be more effective anticancer agents compared to silybin on the cancer cell lines tested, hence validating our approach. The lead compound **15k**, that was identified in this study was found to be effective ($IC_{50} < 1\mu M$, for OV2008 and A2780 cell lines) that's over 30-200 fold compared to silybin ($IC_{50} \sim 30-200 \mu M$). Even more interesting are the findings that **15k** is 6-30 folds more selective to ovarian cancer cells compared to other cancer and normal cells. In the preliminary investigation of **15k's** mechanism of action, we found that **15k** arrests the cell cycle at sub-G1 phase, resulting in loss of mitochondrial membrane potential and thus inducing apoptosis. Further, **15k** binds effectively to the tubulin binding pocket, decreasing the expression and inhibiting tubulin protein function, suggesting that **15k** could be a promising novel inhibitor of tubulin. Further mechanistic studies in cell lines followed by appropriate animal models as proposed here are required to determine the exact mechanisms of action of **15k**. Particularly, the antiproliferative effects of **15k** on the advanced cancers, its ability to reverse metastasis as well as multidrug resistance and its effectiveness as

chemoadjuvant are currently being evaluated in our laboratory and the findings will be reported in due course.

4. Experimental

4.1. Chemistry

All reagents and solvents were obtained from commercial sources and used without further purification unless otherwise specified. The progress of reactions was monitored by thin layer chromatography (TLC) on precoated silica gel F254 plates (Merck) and the spots were visualized by exposure to UV light and/or Iodine vapor. All compounds were obtained in moderate to good yields and purified by column chromatography using Merck 60–120 mesh silica gel. Melting points were determined using an Electrothermal Melting point apparatus and are uncorrected. IR spectra were recorded on a Perkin-Elmer FT-IR spectrometer. ^1H NMR spectra were obtained with a Bruker AM 300 and 400 MHz spectrometer. The chemical shifts are reported in parts per million (δ) downfield using tetramethylsilane as internal standard and CDCl_3 or deuterated DMSO as the solvent. Spin multiplicities are given as s (singlet), d (doublet), m (multiplet) and q (quartet). Coupling constants (J values) were measured in hertz (Hz). ESI MS spectra were recorded on Micromass Quattro II triple quadrupole mass spectrometer. Combustion analyses were performed with Carlo-Erba CHNS-O EA 1108 Elemental Analyser. All the compounds gave satisfactory combustion analysis results (C, H, N within 0.3% of calculated values). The starting material 3-Benzyloxy benzaldehyde was prepared according to the procedure reported in the literature.

4.1.1 Synthesis of 3-(benzyloxy)benzaldehyde (13)

A suspension of 3-hydroxy benzaldehyde **11**, benzyl chloride **12**, K₂CO₃ and KI in 50 ml of EtOH was refluxed for 4.5 hrs. After cooling the solid thus obtained was filtered and washed several times with H₂O. The crude product was purified by column chromatography.

Yield, 79%; dull white solid; m.p. 77–78°C; R_f = 0.61.

4.1.2. General Procedure for synthesis of various substituted (E)-3-(3-(benzyloxy)phenyl)-1-phenylprop-2-en-1-ones (15a–15k)

Equimolar mixture of 3-(benzyloxy)benzaldehyde (**13**) and substituted acetophenones (**14a–14k**) was reacted in the presence of 50% (w/v) KOH/H₂O using ethanol as a solvent. The reaction mixture was stirred at room temperature for 8–24 hr. The reaction mixture was poured into crushed ice (250 g) and left for few hours. To this solution/suspension 1N HCl (10 mL), was added until the solution was acidic. The resulting crude solid precipitate was collected by filtration and dried. Purification was done by recrystallization in CH₃OH or a mixture of CH₃OH and EtOAc with acceptable yields ranging from 70–85%.

(E)-3-(3-(benzyloxy)phenyl)-1-phenylprop-2-en-1-one (15a)

Yield, 85%; dull white solid; mp. 81–82°C; IR ν_{\max} (KBr, cm⁻¹) 1664 (C=O), 1596 (C=C), 1249, 1023 (C–O), 847; ¹H NMR (400 MHz, CDCl₃) δ 8.02 (d, *J* = 7.2 Hz, 2H), 7.78 (d, *J* = 16 Hz, 1H), 7.74 (d, *J* = 16 Hz, 1H), 7.66 (t, *J* = 7.2 Hz, 1H), 7.51–7.61 (m, 5H), 7.32–7.49 (m, 5H), 7.05 (d, *J* = 7.6 Hz, 1H), 5.12 (s, 2H); ¹³C NMR (100 MHz, CDCl₃) δ 190.51, 159.17, 144.68, 138.20, 136.67, 136.35, 132.83, 130.01, 128.69, 128.65, 128.52, 128.14, 127.52, 122.44, 121.44, 117.12, 114.49, 70.19; ESIMS (*m/z*): 315 (M+1); Anal. Calculated for C₂₂H₁₈O₂: C, 84.05; H, 5.77; Found: C, 84.08; H, 5.75.

(E)-3-(3-(benzyloxy)phenyl)-1-(4-chlorophenyl)prop-2-en-1-one (15b)

Yield, 73%; white solid; mp.79–80°C; IR v_{\max} (KBr, cm $^{-1}$) 1679 (C=O), 1592 (C=C), 1258, 1037 (C–O), 828 (Ar); ^1H NMR (400 MHz, CDCl $_3$) δ 7.96 (d, J = 7.2 Hz, 2H), 7.85 (d, J = 16 Hz, 1H), 7.74 (d, J = 16 Hz, 1H), 7.66 (t, J = 7.2 Hz, 1H), 7.32–7.51 (m, 4H), 7.23–7.25 (m, 5H), 7.06 (d, J = 7.6 Hz, 1H), 5.12 (s, 2H); ^{13}C NMR (100 MHz, CDCl $_3$) δ 189.12, 159.19, 145.18, 139.27, 136.62, 136.48, 136.14, 130.06, 129.93, 128.97, 128.70, 128.16, 127.52, 121.84, 121.49, 117.27, 114.58, 70.21; ESIMS (m/z): 349 (M+1); Anal. Calculated for C $_{22}$ H $_{17}$ ClO $_2$: C, 75.75; H, 4.91; Found: C, 75.77; H, 4.95.

(E)-3-(3-(benzyloxy)phenyl)-1-(2,4-dichlorophenyl)prop-2-en-1-one (15c)

Yield, 76%; white solid; mp.64–65°C; IR v_{\max} (KBr, cm $^{-1}$) 1669 (C=O), 1594 (C=C), 1250, 1032 (C–O), 826 (Ar); ^1H NMR (400 MHz, CDCl $_3$) δ 7.51 (d, J = 7.2 Hz, 2H), 7.48 (d, J = 16 Hz, 1H), 7.45 (d, J = 16 Hz, 1H), 7.36 (t, J = 7.2 Hz, 1H), 7.30–7.36 (m, 4H), 7.03–7.17 (m, 4H), 6.99 (d, J = 7.6 Hz, 1H), 5.09 (s, 2H); ^{13}C NMR (100 MHz, CDCl $_3$) δ 192.49, 159.20, 146.36, 137.44, 137.00, 136.55, 135.69, 132.41, 130.47, 130.23, 130.10, 128.69, 128.61, 127.48, 127.33, 126.16, 121.65, 117.80, 114.45, 70.16; ESIMS (m/z): 383 (M+1); Anal. Calculated for C $_{22}$ H $_{16}$ Cl $_2$ O $_2$: C, 68.94; H, 4.21; Found: C, 68.97; H, 4.24.

(E)-3-(3-(benzyloxy)phenyl)-1-(4-nitrophenyl)prop-2-en-1-one (15d)

Yield, 70%; pale yellow solid; mp.127–128°C; IR v_{\max} (KBr, cm $^{-1}$) 1668 (C=O), 1595 (C=C), 1248, 1026 (C–O), 841 (Ar); ^1H NMR (400 MHz, CDCl $_3$) δ 8.34 (d, J = 7.2 Hz, 2H), 8.12 (d, J = 7.2 Hz, 2H), 7.83 (d, J = 16 Hz, 1H), 7.46 (d, J = 16 Hz, 1H), 7.34–7.39 (m, 3H), 7.26–7.31 (m, 5H), 7.07 (d, J = 7.6 Hz, 1H), 5.12; ^{13}C NMR (100 MHz, CDCl $_3$) δ 188.97, 159.24, 150.11, 146.66, 143.01, 136.53, 135.72, 130.18, 129.42, 128.71, 128.21, 127.50, 123.88, 121.67, 121.63, 117.74, 114.76, 70.24; (s, 2H); ESIMS (m/z): 360 (M+1); Anal. Calculated for C $_{22}$ H $_{17}$ NO $_4$: C, 73.53; H, 4.77; N, 3.90; Found: C, 73.52; H, 4.79; N, 3.93.

(E)-3-(3-(benzyloxy)phenyl)-1-p-tolylprop-2-en-1-one (15e)

Yield, 80%; white solid; mp.102–104°C; IR v_{\max} (KBr, cm $^{-1}$) 1651 (C=O), 1603 (C=C), 1248, 1026 (C–O), 807 (Ar); ^1H NMR (400 MHz, CDCl $_3$) δ 7.94 (d, J = 16 Hz, 1H), 7.85 (d, J = 7.2 Hz, 2H), 7.73 (d, J = 7.2 Hz, 2H), 7.52 (d, J = 16 Hz, 1H), 7.26–7.47 (m, 8H), 7.02 (d, J = 7.6 Hz, 1H), 5.11 (s, 2H); 2.44 (s, 3H); ^{13}C NMR (100 MHz, CDCl $_3$) δ 189.94, 159.17, 144.22, 143.70, 136.70, 136.47, 135.62, 129.99, 129.36, 128.69, 128.14, 127.54, 122.45, 121.40, 116.99, 114.48, 70.19, 21.71; ESIMS (m/z): 329 (M+1); Anal. Calculated for C $_{23}$ H $_{20}$ O $_2$: C, 84.12; H, 6.14; Found: C, 84.13; H, 6.18.

(E)-3-(3-(benzyloxy)phenyl)-1-(4-methoxyphenyl)prop-2-en-1-one (15f)

Yield, 81%; white solid; mp.136–138°C; IR v_{\max} (KBr, cm $^{-1}$) 1650 (C=O), 1599 (C=C), 1251, 1023 (C–O), 801 (Ar); ^1H NMR (400 MHz, CDCl $_3$) δ 8.02 (d, J = 7.2 Hz, 2H), 7.73

(d, $J = 16$ Hz, 1H), 7.52 (d, $J = 16$ Hz, 1H), 7.24-7.46 (m, 8H), 6.9–7.06 (m, 3H), 5.11 (s, 2H); 3.89 (s, 3H); ^{13}C NMR (100 MHz, CDCl_3) δ 188.67, 163.47, 159.15, 143.79, 136.70, 136.55, 131.09, 130.84, 129.96, 128.68, 128.13, 127.53, 122.25, 121.34, 116.86, 114.44, 113.87, 70.19, 55.52; ESIMS (m/z): 345 (M+1); Anal. Calculated for $\text{C}_{23}\text{H}_{20}\text{O}_3$: C, 80.21; H, 5.85; Found: C, 84.13; H, 6.18.

(E)-3-(3-(benzyloxy)phenyl)-1-(2,3,4-trichlorophenyl)prop-2-en-1-one (15g)

Yield, 86%; yellow solid; mp. 134–136°C; IR_{vmax} (KBr, cm^{-1}) 1669 (C=O), 1661 (C=C), 1253, 1028 (C–O), 804 (Ar); ^1H NMR (400 MHz, CDCl_3) δ 7.50 (d, $J = 7.2$ Hz, 1H), 7.34–7.44 (m, 5H), 7.26–7.33 (m, 3H), 7.15–7.16 (m, 2H), 7.00–7.06 (m, 2H), 5.09 (s, 2H); ^{13}C NMR (100 MHz, CDCl_3) δ 192.16, 159.21, 147.05, 139.33, 136.50, 136.05, 135.47, 132.92, 131.40, 128.69, 128.65, 128.17, 127.47, 126.98, 126.01, 121.71, 118.03, 114.45, 70.17; ESIMS (m/z): 417 (M+1); Anal. Calculated for $\text{C}_{22}\text{H}_{15}\text{Cl}_3\text{O}_2$: C, 63.26; H, 3.62; Found: C, 63.29; H, 3.66.

(E)-3-(3-(benzyloxy)phenyl)-1-(2-bromophenyl)prop-2-en-1-one (15h)

Yield, 89%; white solid; mp. 84–86°C; IR_{vmax} (KBr, cm^{-1}) 1672 (C=O), 1659 (C=C), 1258, 1021 (C–O), 807 (Ar); ^1H NMR (400 MHz, CDCl_3) δ 7.64 (d, $J = 7.2$ Hz, 2H), 7.28–7.43 (m, 8H), 7.08–7.16 (m, 3H), 7.01 (d, $J = 7.6$ Hz, 2H), 5.07 (s, 2H); ^{13}C NMR (100 MHz, CDCl_3) δ 194.65, 159.18, 146.45, 141.13, 136.58, 135.84, 133.47, 131.43, 130.06, 129.22, 128.68, 128.15, 127.49, 127.39, 126.43, 121.63, 119.53, 117.69, 114.39, 70.14; ESIMS (m/z): 393 (M+1); Anal. Calculated for $\text{C}_{22}\text{H}_{17}\text{BrO}_2$: C, 67.19; H, 4.36; Found: C, 67.15; H, 4.39.

(E)-3-(3-(benzyloxy)phenyl)-1-(3-bromophenyl)prop-2-en-1-one (15i)

Yield, 78%; dull white solid; mp. 110–112°C; IR_{vmax} (KBr, cm^{-1}) 1668 (C=O), 1639 (C=C), 1254, 1021 (C–O), 805 (Ar); ^1H NMR (400 MHz, CDCl_3) δ 8.12 (t, 1H), 7.92–7.89 (d, $J = 7.2$ Hz, 1H), 7.74–7.78 (d, $J = 7.2$ Hz, 1H), 7.63–7.66 (dd, 1H), 7.19–7.45 (m, 10H), 7.02–7.05 (dd, 1H), 5.10 (s, 2H); ^{13}C NMR (100 MHz, CDCl_3) δ 197.04, 159.19, 145.56, 139.98, 136.94, 136.05, 135.67, 131.53, 131.22, 130.26, 130.09, 129.81, 128.60, 128.19, 127.60, 127.54, 126.88, 123.01, 120.09, 117.44, 114.59, 70.22; ESIMS (m/z): 393 (M+1); Anal. Calculated for $\text{C}_{22}\text{H}_{17}\text{BrO}_2$: C, 67.19; H, 4.36; Found: C, 67.17; H, 4.33.

(E)-3-(3-(benzyloxy)phenyl)-1-(4-bromophenyl)prop-2-en-1-one (15j)

Yield, 76%; dull white solid; mp. 112–114°C; IR_{vmax} (KBr, cm^{-1}) 1658 (C=O), 1599 (C=C), 1251, 1026 (C–O), 807 (Ar); ^1H NMR (400 MHz, CDCl_3) δ 7.88 (d, $J = 7.2$ Hz, 2H), δ 7.78 (d, $J = 16$ Hz, 1H), δ 7.64 (d, $J = 7.2$ Hz, 2H), 7.22–7.45 (m, 9H), 7.05 (d, $J = 7.6$ Hz, 1H), 5.11 (s, 2H); ^{13}C NMR (100 MHz, CDCl_3) δ 189.32, 159.19, 145.25, 136.90, 136.63, 136.13, 131.96, 130.05, 128.70, 128.17, 127.95, 127.52, 121.81, 121.50,

117.30, 114.58, 70.21; ESIMS (m/z): 393 (M+1); Anal. Calculated for C₂₂H₁₇BrO₂: C, 67.19; H, 4.36; Found: C, 67.22; H, 4.38.

(E)-3-(3-(benzyloxy)phenyl)-1-(4-hydroxyphenyl)prop-2-en-1-one (15k)

Yield, 84%; yellow solid; mp.129–131°C; IR_{vmax} (KBr, cm⁻¹)1659 (C=O),1598 (C=C), 1254,1022 (C–O),808 (Ar); ¹H NMR (400 MHz, DMSO) δ 8.01 (d, *J* = 7.2 Hz, 2H),7.75 (d, *J* = 16 Hz, 1H),7.67 (d, *J* = 16 Hz, 1H), 7.28-7.48 (m, 7H), 6.9–7.04 (m, 3H), 5.14 (s, 2H); 5.02 (s, 2H); ¹³C NMR (100 MHz, DMSO-d₆) δ 191.89, 158.75, 142.44, 137.42, 136.56, 136.14, 130.79, 129.95, 128.92, 128.17, 127.70, 127.49, 127.30, 122.70, 121.39, 116.68, 69.52 ESIMS (m/z): 331 (M+1); Anal. Calculated for C₂₂H₁₈O₃: C, 79.98; H, 5.49; Found: C, 79.95; H, 5.52.

4.1.3. Procedure for synthesis of unsubstituted (E)-Chalcone (17)

Equimolar mixture of benzaldehyde (**16**) and substituted acetophenone (**14a**) was reacted in the presence of 50% (w/v) NaOH/H₂O using ethanol as a solvent. The reaction mixture was stirred at room temperature for 2 hr. The reaction mixture was poured into crushed ice (250 g) and left for few hours. To this solution/suspension 1N HCl (10 mL), was added until the solution was acidic. The resulting crude solid precipitate was collected by filtration and dried. Purification was done by recrystallization in CH₃OH with excellent yields.

Yield, 85%; Yellow solid; mp.56–58°C; IR_{vmax} (KBr, cm⁻¹) 1661 (C=O), 1605 (C=C), 1248, 1020 (C–O), 746 (Ar); ¹H NMR (400 MHz, CDCl₃) δ 8.01 (m, 2H), 7.92 (d, *J* = 16 Hz, 1H), 7.77 (d, *J* = 16 Hz, 1H), 7.55 (m, 8H).ESIMS (m/z): 209 (M+1); Anal. Calcd for C₁₅H₁₂O: C,86.51; H, 5.81; Found: C, 86.50; H, 5.84.

4.2. Biological studies

4.2.1 Reagents:

The antibodies α- tubulin and β- actin were purchased from Cell Signalling Technology (Danvers, MA, USA). A Mitochondrial Membrane Potential/Annexin V apoptosis Kit, Propidium iodide dye were purchased from life technologies (Eugene, Oregon, USA).

Dulbecco's modified Eagle medium (DMEM) was purchased from GE Healthcare Life Sciences, HyClone Laboratories (Logan, Utah, USA).

4.2.2. Cell lines and cell culture

A panel of different cancer cell lines, including breast (MCF7, ZR-75-1, MDAMB231, BT20), ovarian (A2789, OV2008), pancreatic (PANC1), and prostate (DU-145) cancer cell lines, as well as normal cell lines (Chinese hamster ovarian: CHO; human epithelial normal colon: CRL 1459; human embryonic kidney: HEK293), were grown as adherent monolayers in flasks with DMEM supplemented with 10% fetal bovine serum (FBS) in a humidified incubator with 5% CO₂ at 37°C.

4.2.3 Cell cytotoxicity by MTT assays and morphological analysis:

The (3-(4,5-dimethylthiazol-2-yl)-2,5-diphenyltetrazolium bromide) (MTT) assay was used to determine the cytotoxicity of the twelve silybin derivative compounds in the above mentioned cell lines. Briefly, cells were harvested with 0.25% trypsin, 2.21 mM EDTA, 1X from Corning (Corning, NY 14831USA) and suspended at a final concentration of 5×10^3 cells/well. Cells were seeded (180 μ L/well) into 96-well multiplates. To the seeded cells eight different concentrations of each derivative in the series (20 μ L) were added at 0, 0.1, 0.3, 1, 3, 10, 30, and 100 μ M. After 68h of incubation, 20 μ L of MTT solution (4 mg/mL) was added to each well, and the plates were incubated for 4h. This allowed viable cells to convert the yellow-colored MTT into dark-blue formazan crystals. Subsequently, the medium was discarded, and 100 μ L of

DMSO was added into each well to dissolve the formazan crystals. The absorbance was determined at 570 nm with a DTX 880 multimode detector (Beckman Coulter life sciences, IN, USA). The $IC_{50} \pm SD$ concentrations were calculated from three experiments performed in triplicate. The IC_{50} values were calculated from the cell survival percentages obtained for each compound tested at eight different concentrations. Similarly, the cytotoxicity of the test compounds was compared to the normal cell lines (CHO, CRL 1459 and HEK293).

4.2.4 Confluence with time analysis

OV2008, A2780 cells were seeded in low density (1×10^3) cell/ well in 96 well plates. Compound **15k** was added in different concentrations (0, 2, 4, and 8) μ M and incubated in the IncuCyte ZOOM® System (Essen BioScience, Inc., Ann Arbor, MI, USA). This live cell imaging system allowed the imaging of the cells every two hours for up to 48 h. The cells confluences at each time point were analyzed using the IncuCyte associated analysis system. A blue confluence mask was added to the cells and timeline curves were drawn for each concentration. The data is presented as means \pm SD of three independent experiments.

4.2.5 Cell cycle analysis:

Cell cycle analysis was performed as previously described [4]. Briefly, OV2008 cells were plated into 6 well plates at 1×10^6 cells/ well. The cells were incubated with 0, 2 or 4 μ M of **15k** compound and incubated for 12 h. Next, the cells were trypsinized with

.25% trypsin, 2.21 mM EDTA, 1X, washed, counted and resuspended in 0.5ml ice cold PBS. The cells then were stained with propidium iodide (PI) dye and incubated for at least 15 minutes. The distribution of the cells in each cell cycle phase for the different compounds was measured using BD Accuri™ C6 flow cytometer from BD Biosciences (Becton-Dickinson, San Jose, CA, USA) and analysed using FCS express 5 plus De Novo software (Glendale, CA, USA).

4.2.6 Apoptosis and mitochondrial membrane potential analysis:

MitoTracker Red and Alexa Fluor 488 annexin V kits for flow cytometry (Molecular Probes Inc., Invitrogen, Eugene, OR) were used to measure mitochondrial membrane potential and apoptosis, respectively, in OV2008 cells. Briefly, cells were seeded in 6 well plates and treated with 0, 2, or 4 μM of compound **15k** for 12 h. The cells were then trypsinized 0.25% trypsin, 2.21 mM EDTA, 1X, counted, and 4 μl of 10 μM MitoTracker Red working solution was added to 1 ml of the harvested cells. The cells were incubated at 37 °C with 5% CO₂ for 30 minutes. Next, PBS washing was followed by cells resuspension in 100 μl of annexin binding buffer. The cell suspensions were then incubated with 5 μl of Alexa Fluor 488 annexin V for 15 minutes. This was followed by adding 400 μl of annexin-binding buffer. Finally, flow cytometry was used to detect the stained cells and fluorescence emission at 530 nm and 585 nm was used with the BD Accuri™ C6 flow cytometer from BD Biosciences (Becton-Dickinson, San Jose, CA, USA) and analysed using FCS express 5 plus De Novo software (Glendale, CA, USA).

4.2.7 Protein expression analysis using Western blot:

To measure the expression of α -tubulin, β -actin proteins, Western blotting was performed by lysing OV2008 cell lines using a lysis buffer (50 mM Tris-HCl, 150 mM NaCl, 1 mM EDTA, 0.5% NP-40, 1% Triton, 0.1% SDS) containing a protease inhibitor cocktail from sigma-Aldrich life science (St. Louis, MO, USA). Bicinchoninic acid (BCA) quantification assay was used to determine protein amount in the cell extracts (G-BIOSCIENCES, St. Louis, MO, USA). The extracted proteins were loaded onto a 10-20% tris-glycine gel. After separation, proteins were transferred from the gel onto a PVDF membrane. Membranes were blocked using 5% milk in Tris-buffered saline Tween 20 for 30 minutes. Rabbit α -tubulin (Cell signalling technology; 1:3000 dilution and rabbit actin antibody (Covance; 1:5000 dilutions) were added to the blocking buffer, and the membrane was incubated overnight at 4 °C. Membranes were washed and incubated with horseradish peroxidase-labelled (HRP) anti-rabbit secondary antibody (1:5000 dilutions). The membrane was incubated with the antibody for additional 1 hour. Subsequently, membranes were washed and developed by Clarity Western ECL substrate (Bio-Rad; Hercules, California, USA). Protein was detected using ChemiDoc Imaging System (Bio-Rad). Densitometry analyses of the blots for the detected protein were quantified using the image J software. Data was calculated as ratios of α -tubulin / β -actin.

4.2.8 Immunofluorescence imaging analysis:

To measure the expression of α -tubulin, OV2008 cells were seeded in a density of 4×10^4 cell/ well and allowed to grow overnight. Cells were then incubated with different concentrations of the synthetic derivatives for 24h at 37°C. The cells that had been

incubated with the test compounds were fixed with 4% paraformaldehyde, followed by permeabilization with Triton 100x 0.3% in PBS for 25 minutes. Subsequently, the cells were blocked with 3% BSA in PBS for at least 30 minutes. The α - tubulin rabbit antibody, in the correct dilution, was added followed by anti-Rabbit IgG (H+L), F(ab')₂ Fragment (Alexa Fluor® 488 Conjugate) (green) in a similar fashion. Finally, to color the nucleus of each cell, the propidium iodide stain was added to each slide. The slides were allowed to dry for at least one hour and the fluorescence was detected under a fluorescent microscope (EVOS cell imaging system) (Thermofisher scientific, Wayne, MI, USA).

4.3 Molecular Docking Studies

Ligand structure preparation

The structure of the ligand **15k** was constructed using the builder module of Maestro v 9.3.5 and subsequently prepared using the Ligprep (ver 2.5) module of the Schrödinger Suite. Ligprep modifies the bond orders according to their data and generates different conformers for the input structures. Each generated conformer was subjected to energy minimization with OPLS (Optimized Potential for liquid Simulations) force field to eliminate the bond length and bond angles biased from the crystal structure[60]. Finally, Ligprep produces structures with various ionization states, tautomers, stereochemistries, and ring conformations. The ligand (**15k**) structures obtained from the LigPrep v2.5 run were used for generating 100 ligand conformations for each structure, using the default parameters of mixed torsional/low-mode sampling. The

output conformational search (Csearch) file containing 100 unique conformers of **15k** was given as input for docking simulations at the colchicine-binding site of tubulin.

Protein structure preparation

The crystal structure of tubulin (PDB code: 1SA0), obtained from the Protein Data Bank at the Research Collaboratory for Structural Bioinformatics (RCSB) (<http://www.rcsb.org>), was used as a target for the molecular docking studies. The protein model was optimized using the 'Protein Preparation Wizard' workflow implemented in the Schrödinger molecular modelling suite (Schrödinger, Inc., New York, NY, 2012). This optimization includes adding hydrogen atoms, assigning correct bond orders and building disulfide bonds. The protonation states of all of the ionizable residues were predicted by PROPKA provided in the protein preparation wizard. An optimized structure model was energy minimized (only hydrogen atoms) using the OPLS2005 force field. The colchicine binding site present in refined protein model of tubulin was used to generate grid for docking the ligands.

Docking protocol

The diverse conformational library of **15k** was docked at the generated grid using the "Extra Precision" (XP) mode of Glide program v5.8 (Schrödinger, Inc., New York, NY, 2012) with the default functions. The best docked conformations of **15k** as established by high XP GScore were chosen and used for further analysis. All

computations were carried out on a Dell Inspiron Core i3 processor workstation with Windows 7 operating system.

2.4 Statistical analysis:

All of the experiments were done in triplicate. Two-way ANOVA, One-way ANOVA and Student's t-test were used to compare different treatment groups (GraphPad Prism, version 5.04). The results were presented as the mean \pm standard deviation (SD), with a priori significance level of $p < 0.05$.

Acknowledgements

This research was supported by CAYT scheme, All India Council for Technical Education, Govt. of India (to E.M.). Authors are grateful to SAIF, CDRI, Lucknow and IIT, Indore for providing analytical spectral data. This work was also funded by the University of Toledo start-up grant (F110760) to A.K.T. We would like to thank Dr. Charles Jr. Ashby (St. John's University, NY) and Charisse Montgomery (University of Toledo) for editorial assistance.

Conflict of Interest:

Authors declare no conflict of interest.

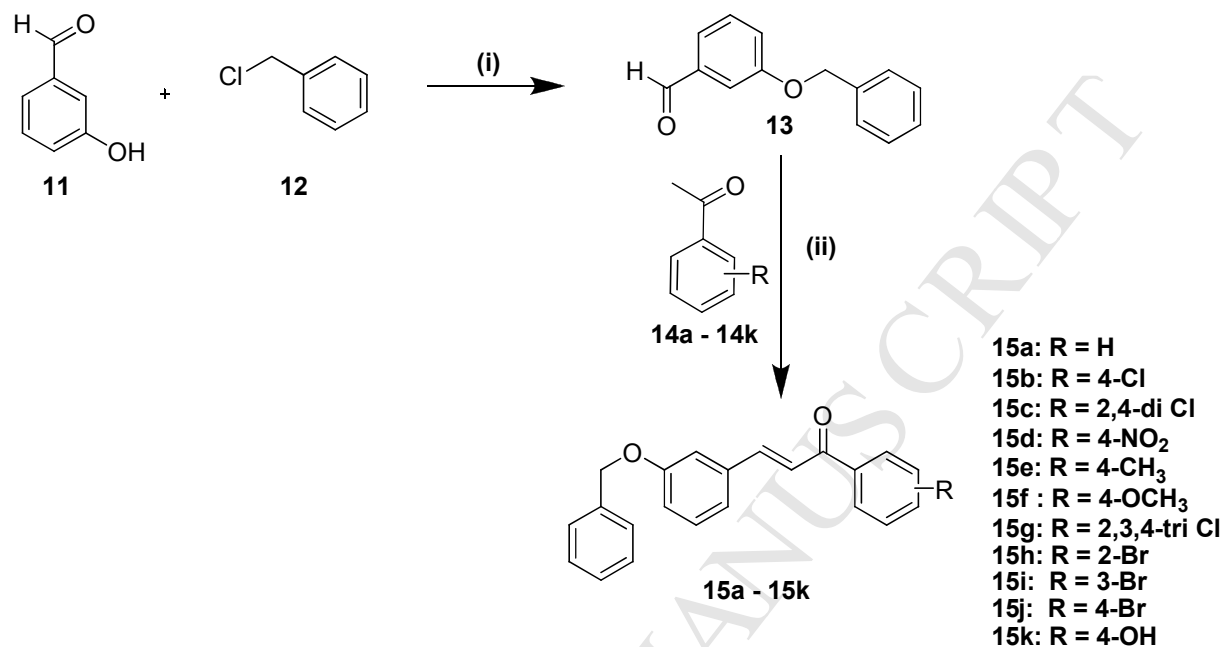
Table 1: The effects of the silybin derivatives on the survival of cancer cell lines (breast, prostate, pancreatic and ovarian) and normal non-cancerous cell lines (normal epithelial colon, kidney and ovarian).

Compound Code	Breast Cancer				Prostate Cancer	Pancreatic Cancer
	MCF-7	ZR-75-1	BT-20	MDA-MB231	DU-145	PANC1

15a	9.8 ± 3.0	8.5 ± 0.9	25.5 ± 0.2	20.0 ± 1.9	42.4 ± 7.1	23.5 ± 1.7
15b	24.8 ± 2.3	20.0 ± 2.1	63.2 ± 1.3	21.5 ± 1.0	43.4 ± 4.0	21.3 ± 3.1
15c	9.4 ± 0.5	9.4 ± 0.9	19.2 ± 1.8	6.8 ± 2.1	27.3 ± 2.0	27.2 ± 2.1
15d	17.5 ± 2.8	37.7 ± 1.1	80.9 ± 8.6	23.3 ± 2.3	52.5 ± 3.1	25.4 ± 1.1
15e	21.7 ± 1.1	25.8 ± 4.2	61.0 ± 3.5	15.6 ± 2.3	25.6 ± 3.5	41.6 ± 1.6
15f	6.0 ± 0.9	19.9 ± 1.2	38.3 ± 5.1	12.4 ± 1.4	51.3 ± 1.9	44.3 ± 1.4
15g	2.4 ± 0.5	6.2 ± 0.0	3.9 ± 0.9	2.4 ± 0.1	6.4 ± 0.5	2.4 ± 0.4
15h	1.6 ± 0.9	2.9 ± 0.1	1.8 ± 0.9	1.8 ± 0.4	3.0 ± 1.1	61.2 ± 1.2
15i	7.9 ± 1.1	8.3 ± 0.1	7.1 ± 0.8	6.9 ± 1.0	9.1 ± 0.9	6.4 ± 0.3
15j	6.5 ± 1.5	6.5 ± 0.1	7.4 ± 0.5	6.4 ± 0.3	5.7 ± 0.7	2.1 ± 0.6
15k	2.8 ± 0.9	4.9 ± 0.2	5.1 ± 2.1	2.9 ± 0.6	6.3 ± 1.0	2.6 ± 0.9
17	12.6 ± 1.5	13.7 ± 0.9	21.1 ± 0.9	6.7 ± 1.0	50.1 ± 1.1	26.0 ± 2.3
Compound Code	Ovarian Cancer			Normal Cells		
	OV2008	A2780	CRL-1459	HEK-293	CHO	
15a	4.9 ± 1.4	6.7 ± 0.7	7.8 ± 1.0	14.1 ± 3.6	22.0 ± 1.7	
15b	20.0 ± 2.3	56.4 ± 2.8	12.8 ± 2.1	22.8 ± 1.5	43.6 ± 1.9	
15c	5.2 ± 1.1	21.4 ± 3.2	7.8 ± 1.1	24.9 ± 3.2	27.5 ± 1.2	
15d	49.0 ± 1.0	56.4 ± 4.6	26.0 ± 1.6	59.3 ± 5.9	82.4 ± 1.7	
15e	12.9 ± 0.9	20.5 ± 1.9	19.8 ± 1.3	8.2 ± 0.5	26.4 ± 0.9	
15f	17.2 ± 1.0	38.1 ± 2.8	25.4 ± 1.9	79.8 ± 2.8	22.9 ± 0.3	
15g	1.5 ± 0.9	1.5 ± 0.0	2.5 ± 0.2	2.4 ± 0.5	8.6 ± 0.9	
15h	1.2 ± 0.4	2.5 ± 0.0	2.4 ± 0.9	2.2 ± 0.0	9.1 ± 0.2	
15i	5.7 ± 0.1	6.3 ± 1.0	7.2 ± 0.9	7.1 ± 1.3	9.2 ± 0.4	
15j	1.0 ± 0.1	1.8 ± 0.1	5.3 ± 1.0	5.4 ± 0.9	9.0 ± 0.5	
15k	0.8 ± 0.1	1.0 ± 0.1	8.5 ± 0.7	5.4 ± 0.9	8.1 ± 1.2	
17	33.4 ± 2.1	67.5 ± 4.3	6.4 ± 0.4	10.7 ± 1.8	23.0 ± 1.3	

Cell survival was determined by MTT assay as described in materials and methods. The IC₅₀ values are represented as mean ± SD of three independent experiments performed in triplicate. The compounds were screened on breast (ZR-75-1, BT-20, MDAMB-231 & MCF-7), prostate (DU-145), pancreatic (PANC1), Ovarian (OV2008 & A2780) cancer cell lines and normal cancer cell lines (colon: CRL-1459, human embryonic kidney: HEK-293 and ovarian: CHO).

Scheme1: The synthetic scheme for the novel silybin derivatives **15a – 15k** with aromatic substituent modification. Reagents and conditions: (i) K_2CO_3/KI , $70^\circ C$, 24 h; (ii) 50% w/v KOH/H_2O , RT, 8 h.



Scheme 2: The synthetic scheme for chalcone 17; Reagents and conditions: (i) 50% w/v KOH/H₂O, RT, 1 h

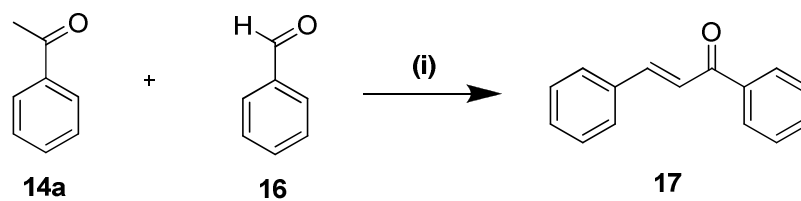


Figure legends:

Figure 1. The chemical structures of the active constituents of Silymarin, the main polyphenolic flavonoid found in the milk thistle plant extract: (silybin A (1), silybin B (2), isosilybin A (3), isosilybin B (4), silychristin (5), isosilychristin (6), silydianin (7) and (+)-taxifoline (8).

Figure 2. Modifications on silybin structure by NLP and ring disjunctive approach to develop novel silybin derivatives.

Figure 3. Cytotoxic effects of **15k** on ovarian cancer cell lines in concentration and time dependent manner are shown. **(A)** Morphological analysis of the cytotoxic effects of **15k** at 0, 1, 2 and 4 μM on ovarian cancer cells, OV2008, A2780 and normal epithelial Chinese hamster ovarian cell line (CHO), exposed for 68 h is shown. The cells were photographed (at 20X) for each triplicate treatment with an inverted microscope (Olympus, BX53F) with fluorescent lamps and digital cameras. A representative figure is shown for each treatment. The data were acquired and analysed with Cell Sens software; **(B)** Survival of ovarian cancer cells OV2008 and A2780 compared to that of CHO; **(C)** IC_{50} values of **15k** for ovarian cancer cells OV2008 and A2780 relative to CHO is shown. Cell survival was determined by the MTT assay. IC_{50} values are represented as means \pm SD of three independent experiments performed in triplicate. Statistically, ***P value < 0.0001 in ovarian cancer cells versus the CHO; **(D) and (F)** a representative images of the proliferation and confluence of OV2008 and A2780 cells respectively at different time points (0, 12, 24, 36, and 48) h at 0 or 2 μM of **15k** is shown. A blue mask was applied by IncuCyte software during the analysis for quantification analysis ; **(E) and (G)** a timeline curve quantitatively showing the % of

confluence in OV2008, A2780 cell lines respectively versus time at different concentrations 0, 2, 4, and 8 μM of **15k** is shown. The data represents means \pm SD of three independent experiments performed in triplicate.

Figure 4. Effects of **15k** on mitochondrial membrane potential, apoptosis and cell cycle
(A) The OV2008 and A2780 cells in complete medium were exposed to **15k** at 0, 2, or 4 μM for 12h. Cells were then treated with the reagents of the MitoTracker Red and Alexa Fluor 488 annexin V kits for flow cytometry. Representative results of OV2008 and A2780 cells respectively from two independent experiments, each performed in triplicate, are shown; **(B)** Histograms quantitatively summarizes the results of **(A)** on OV2008 and A2780 respectively; **(C)** The induction of cell cycle arrest in OV2008 by **15k** is shown. The OV2008 treated with different concentrations (0, 2, 4 μM) of **15k** for 12h was subjected to cell cycle analysis by flow cytometry of PI (X axis)/cell counts(Y axis); **(D)** A histogram quantitatively summarizing the change in % of cells in each phase of the cell cycle due to the treatment with **15k**. The data represents means \pm SD of three independent experiments performed in triplicate.

Figure 5: 15k effects on α - tubulin protein level of expression and binding analysis. **(A)** OV2008 cells were **15k** (0, 2, and 4) μM overnight as described above. Western blot analysis of expression α - tubulin protein level along with quantification of relative expression to β - actin are shown **(B)** Effect of **15k** on spindle microtubule formation in OV2008. Cells were cultured in presence of (0, 2 and 4) μM of **15k** overnight. Cells were then fixed and labelled with a monoclonal α -tubulin (green) antibody conjugated to FITC and nuclei stained with DAPI (blue) as described in materials and methods. Immuno fluorescence analysis of α - tubulin expression levels are shown. **(C)** XP-Glide predicted

binding mode **15k** with α - tubulin protein. The docked conformation of **15k** is shown as ball and stick model within the large hydrophobic cavity of α - tubulin. Important amino acids are depicted as sticks with the atoms colored as follows: carbon = green, hydrogen = white, nitrogen = blue, oxygen = red, and sulfur = yellow, whereas the SDA is shown with the same color scheme as above except the carbon atoms are represented in orange. The dotted red line indicates hydrogen-bonding interactions. **(D)** XP-Glide predicted binding mode colchicine with α - tubulin protein. The docked conformation of colchicine is shown as ball and stick model within the large hydrophobic cavity of α - tubulin. Important amino acids are depicted as sticks with the atoms colored as follows: carbon = green, hydrogen = white, nitrogen = blue, oxygen = red, and sulfur = yellow, whereas the SDA is shown with the same color scheme as above except the carbon atoms are represented in orange. The dotted red line indicates hydrogen-bonding interactions.

Figure 1:

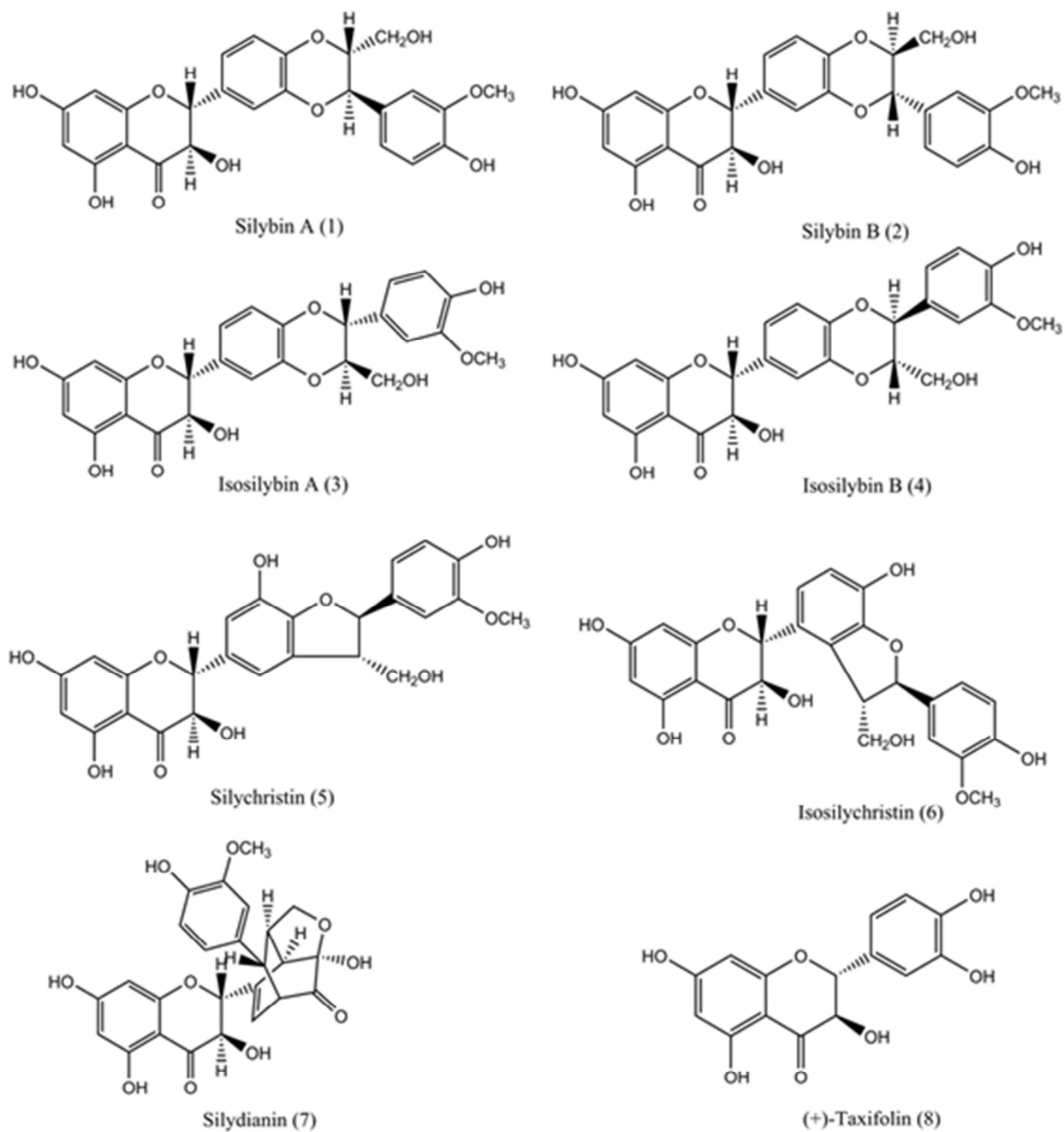


Figure 2.

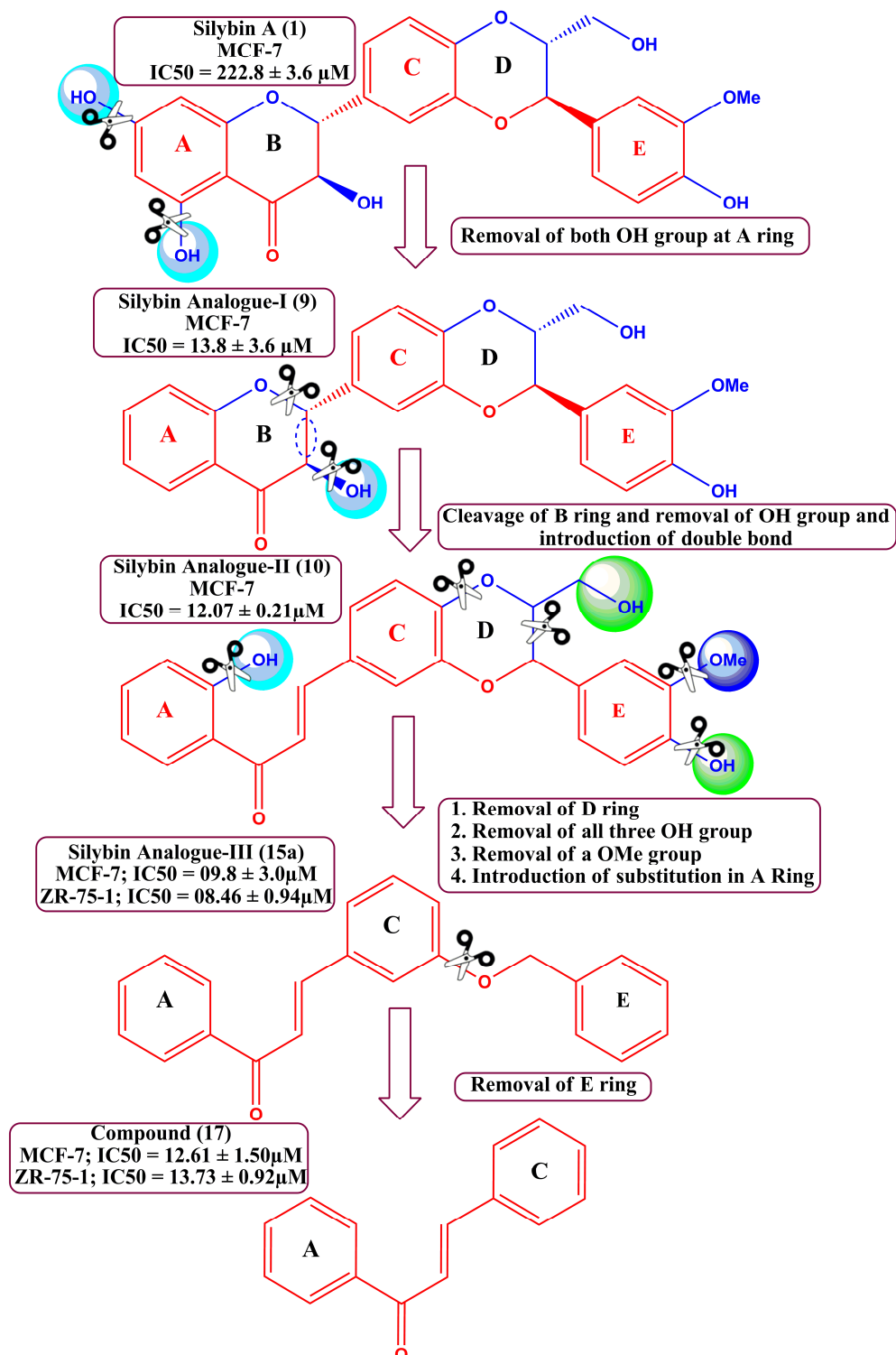


Figure 3.

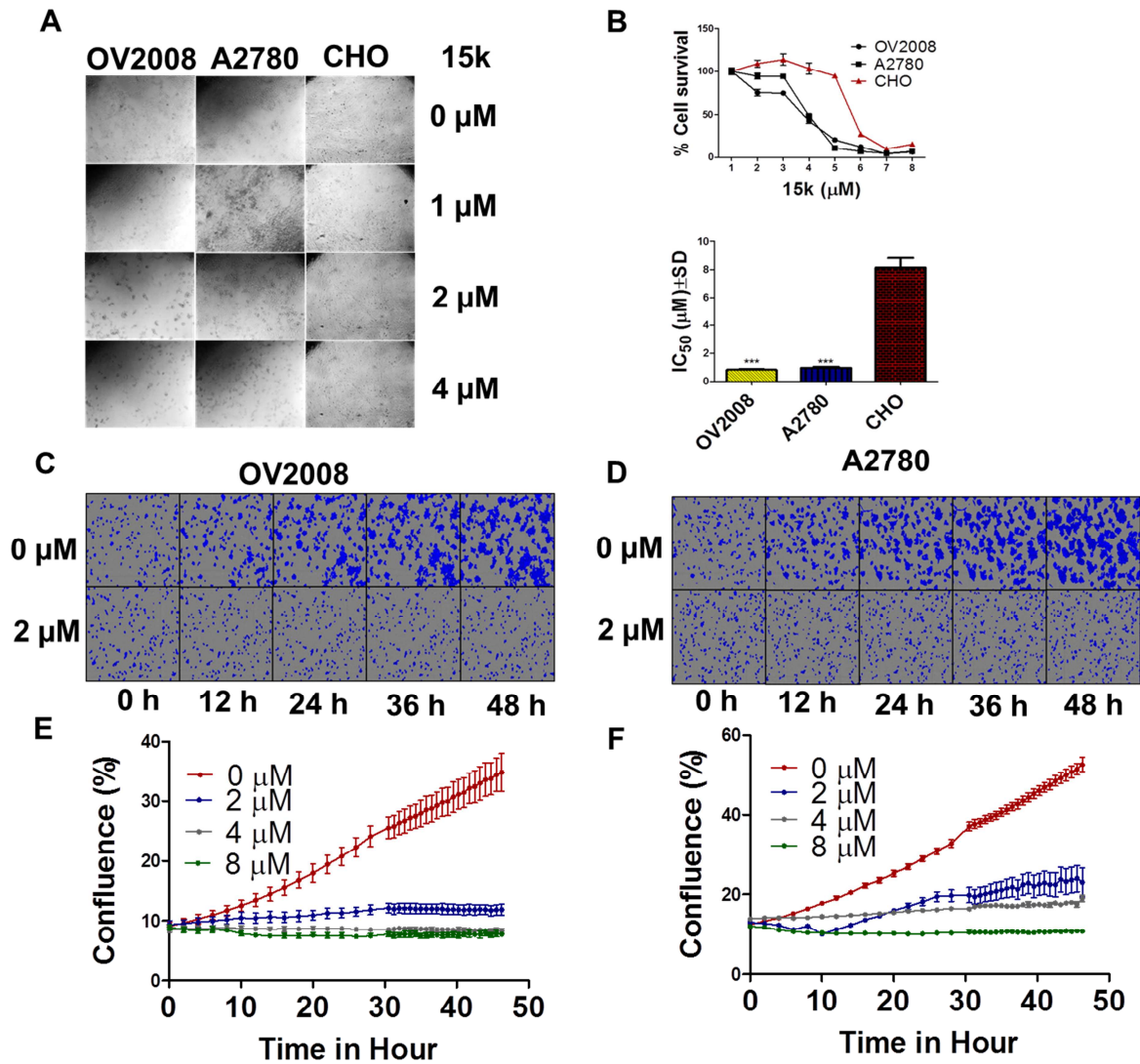


Figure 4.

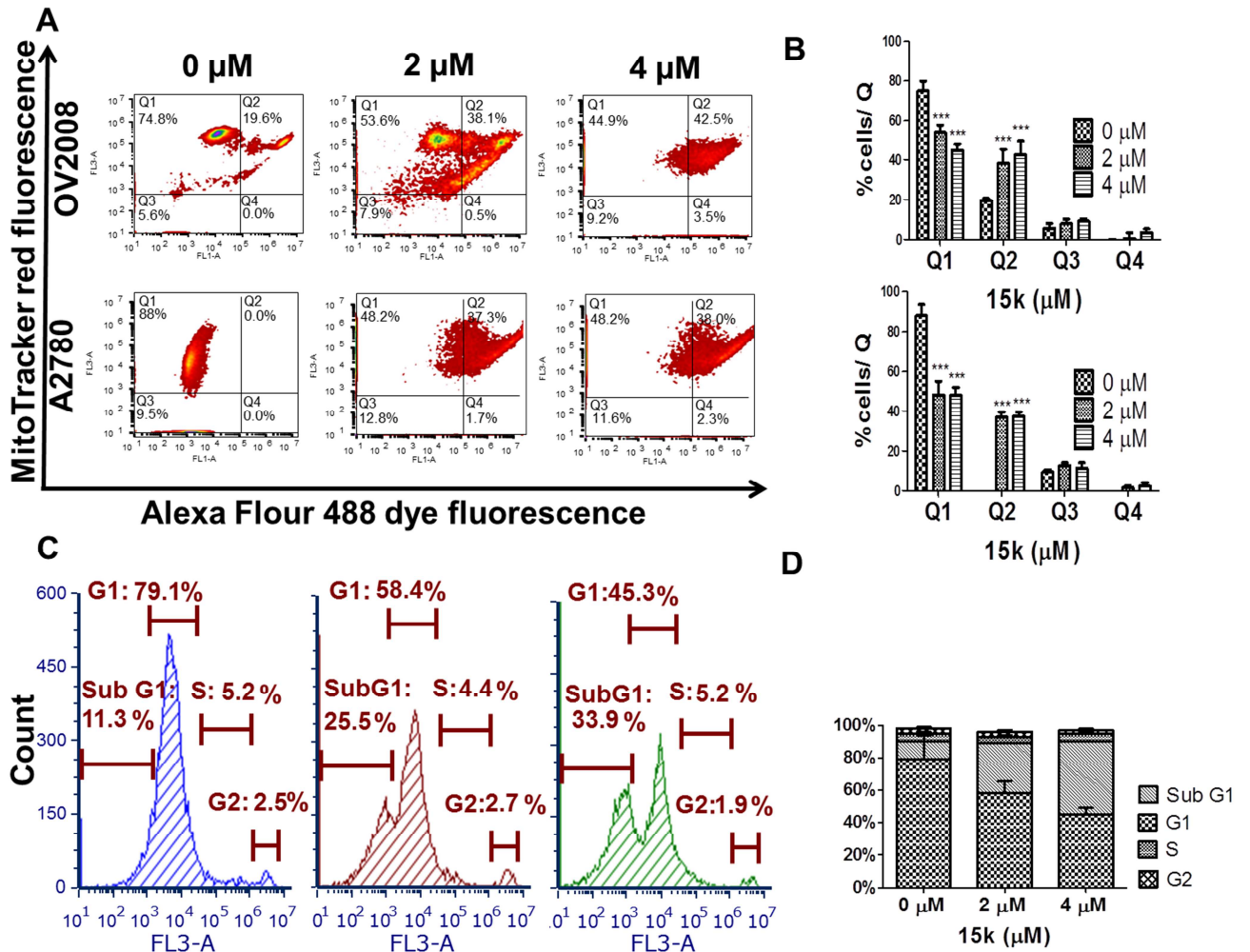
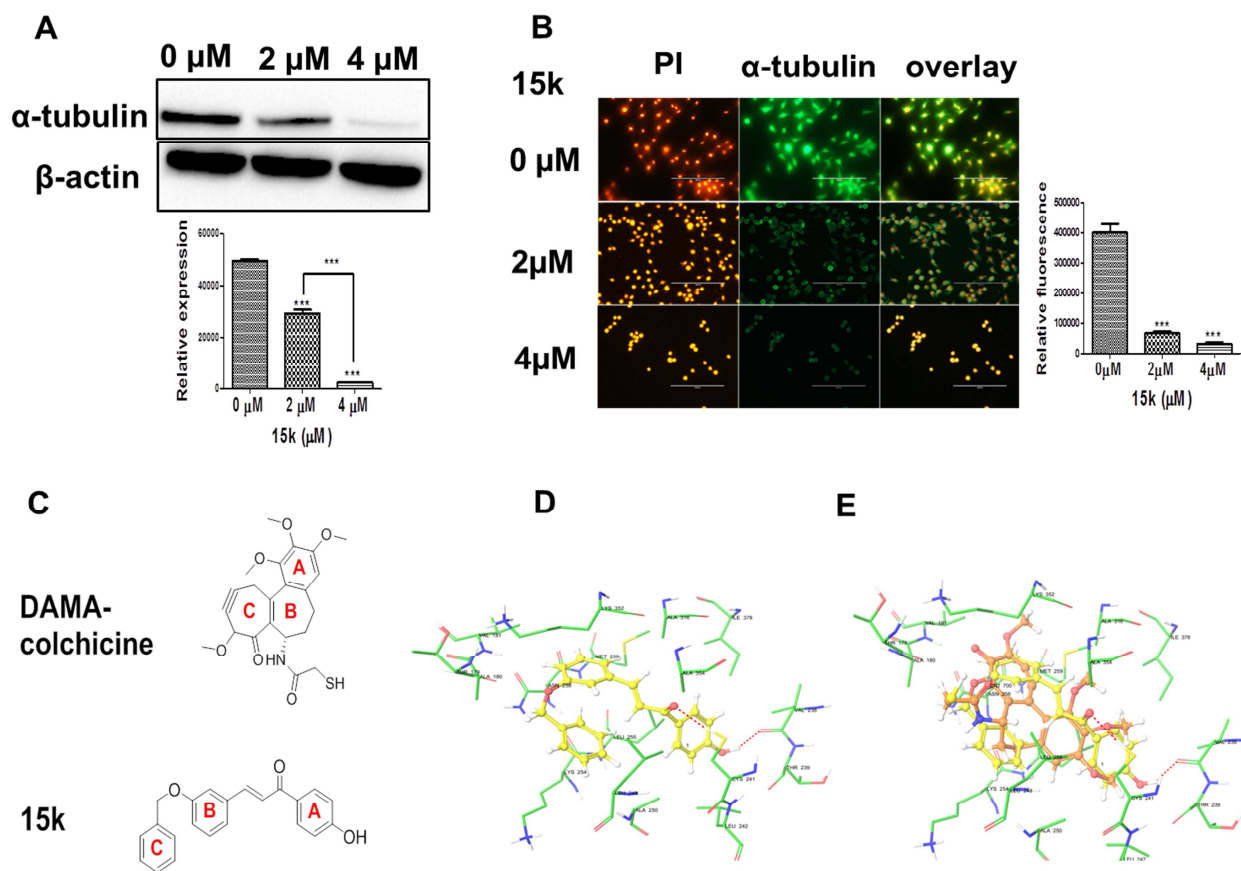


Figure 5.



References

- [1] D.J. Newman, G.M. Cragg, Natural products as sources of new drugs from 1981 to 2014, *Journal of natural products*, 79 (2016) 629-661.
- [2] V. Simanek, V. Kren, J. Ulrichova, J. Vicar, L. Cvak, Silymarin: What is in the name...? An appeal for a change of editorial policy, *Hepatology (Baltimore, Md.)*, 32 (2000) 442-444.
- [3] B.E. 7. Morazzoni P, *Silybum marianum (Carduus marianus)*
Fitoterapia, 66 (1995) 03-49.
- [4] V.L. Nayak, N. Nagesh, A. Ravikumar, C. Bagul, M.V. Vishnuvardhan, V. Srinivasulu, A. Kamal, 2-aryl benzimidazole conjugate induced apoptosis in human breast cancer MCF-7 cells through caspase independent pathway, *Apoptosis : an international journal on programmed cell death*, (2016).
- [5] D. Biedermann, E. Vavrikova, L. Cvak, V. Kren, Chemistry of silybin, *Natural product reports*, 31 (2014) 1138-1157.
- [6] R. Gazak, D. Walterova, V. Kren, Silybin and silymarin--new and emerging applications in medicine, *Current medicinal chemistry*, 14 (2007) 315-338.
- [7] I. Szilagi, P. Tetenyi, S. Antus, O. Seligmann, V.M. Chari, M. Seitz, H. Wagner, [Structure of silandrin and silymonin, two new flavanolignans from a white blooming *Silybum marianum* variety], *Planta medica*, 43 (1981) 121-127.
- [8] N.C. Kim, T.N. Graf, C.M. Sparacino, M.C. Wani, M.E. Wall, Complete isolation and characterization of silybins and isosilybins from milk thistle (*Silybum marianum*), *Organic & biomolecular chemistry*, 1 (2003) 1684-1689.
- [9] D.Y. Lee, Y. Liu, Molecular structure and stereochemistry of silybin A, silybin B, isosilybin A, and isosilybin B, Isolated from *Silybum marianum* (milk thistle), *Journal of natural products*, 66 (2003) 1171-1174.
- [10] H. Wagner, L. Horhammer, R. Munster, [On the chemistry of silymarin (silybin), the active principle of the fruits from *Silybum marianum* (L.) Gaertn. (*Carduus marianus* L.)], *Arzneimittel-Forschung*, 18 (1968) 688-696.
- [11] F. Fraschini, G. Demartini, D. Esposti, Pharmacology of Silymarin, *Clinical Drug Investigation*, 22 (2002) 51-65.
- [12] R. Gažák, K. Purchartová, P. Marhol, L. Živná, P. Sedmera, K. Valentová, N. Kato, H. Matsumura, K. Kaihatsu, V. Křen, Antioxidant and antiviral activities of silybin fatty acid conjugates, *European Journal of Medicinal Chemistry*, 45 (2010) 1059-1067.
- [13] E. Vavříková, V. Křen, L. Jezova-Kalachova, M. Biler, B. Chantemargue, M. Pyszková, S. Riva, M. Kuzma, K. Valentová, J. Ulrichová, J. Vrba, P. Trouillas, J. Vacek, Novel flavanolignan hybrid antioxidants: From enzymatic preparation to molecular rationalization, *European Journal of Medicinal Chemistry*, 127 (2017) 263-274.

- [14] R. Agarwal, C. Agarwal, H. Ichikawa, R.P. Singh, B.B. Aggarwal, Anticancer potential of silymarin: from bench to bed side, *Anticancer research*, 26 (2006) 4457-4498.
- [15] A.K. Tyagi, C. Agarwal, D.C. Chan, R. Agarwal, Synergistic anti-cancer effects of silibinin with conventional cytotoxic agents doxorubicin, cisplatin and carboplatin against human breast carcinoma MCF-7 and MDA-MB468 cells, *Oncology reports*, 11 (2004) 493-499.
- [16] C. Agarwal, R. Wadhwa, G. Deep, D. Biedermann, R. Gazak, V. Kren, R. Agarwal, Anti-cancer efficacy of silybin derivatives -- a structure-activity relationship, *PloS one*, 8 (2013) e60074.
- [17] G. Ramakrishnan, L. Lo Muzio, C.M. Elinos-Baez, S. Jagan, T.A. Augustine, S. Kamaraj, P. Anandakumar, T. Devaki, Silymarin inhibited proliferation and induced apoptosis in hepatic cancer cells, *Cell proliferation*, 42 (2009) 229-240.
- [18] N. Polachi, G. Bai, T. Li, Y. Chu, X. Wang, S. Li, N. Gu, J. Wu, W. Li, Y. Zhang, Modulatory effects of silibinin in various cell signaling pathways against liver disorders and cancer—A comprehensive review, *European Journal of Medicinal Chemistry*, 123 (2016) 577-595.
- [19] K. Ramasamy, R. Agarwal, Multitargeted therapy of cancer by silymarin, *Cancer letters*, 269 (2008) 352-362.
- [20] L. Fan, Y. Ma, Y. Liu, D. Zheng, G. Huang, Silymarin induces cell cycle arrest and apoptosis in ovarian cancer cells, *European journal of pharmacology*, 743 (2014) 79-88.
- [21] G. Deep, N.H. Oberlies, D.J. Kroll, R. Agarwal, Isosilybin B and isosilybin A inhibit growth, induce G1 arrest and cause apoptosis in human prostate cancer LNCaP and 22Rv1 cells, *Carcinogenesis*, 28 (2007) 1533-1542.
- [22] G. Deep, N.H. Oberlies, D.J. Kroll, R. Agarwal, Identifying the differential effects of silymarin constituents on cell growth and cell cycle regulatory molecules in human prostate cancer cells, *International journal of cancer*, 123 (2008) 41-50.
- [23] B. Vue, S. Zhang, X. Zhang, K. Parisi, Q. Zhang, S. Zheng, G. Wang, Q.-H. Chen, Silibinin derivatives as anti-prostate cancer agents: Synthesis and cell-based evaluations, *European journal of medicinal chemistry*, 109 (2016) 36-46.
- [24] R.P. Singh, A.K. Tyagi, J. Zhao, R. Agarwal, Silymarin inhibits growth and causes regression of established skin tumors in SENCAR mice via modulation of mitogen-activated protein kinases and induction of apoptosis, *Carcinogenesis*, 23 (2002) 499-510.
- [25] R.P. Singh, R. Agarwal, Flavonoid antioxidant silymarin and skin cancer, *Antioxidants & redox signaling*, 4 (2002) 655-663.
- [26] X. Zi, H. Mukhtar, R. Agarwal, Novel cancer chemopreventive effects of a flavonoid antioxidant silymarin: inhibition of mRNA expression of an endogenous tumor promoter TNF alpha, *Biochemical and biophysical research communications*, 239 (1997) 334-339.

- [27] S.N. Kang, M.H. Lee, K.M. Kim, D. Cho, T.S. Kim, Induction of human promyelocytic leukemia HL-60 cell differentiation into monocytes by silibinin: involvement of protein kinase C, *Biochemical pharmacology*, 61 (2001) 1487-1495.
- [28] H.G. Yoo, S.N. Jung, Y.S. Hwang, J.S. Park, M.H. Kim, M. Jeong, S.J. Ahn, B.W. Ahn, B.A. Shin, R.K. Park, Y.D. Jung, Involvement of NF-kappaB and caspases in silibinin-induced apoptosis of endothelial cells, *International journal of molecular medicine*, 13 (2004) 81-86.
- [29] N. Bhatia, J. Zhao, D.M. Wolf, R. Agarwal, Inhibition of human carcinoma cell growth and DNA synthesis by silibinin, an active constituent of milk thistle: comparison with silymarin, *Cancer letters*, 147 (1999) 77-84.
- [30] S.K. Manna, A. Mukhopadhyay, N.T. Van, B.B. Aggarwal, Silymarin suppresses TNF-induced activation of NF-kappa B, c-Jun N-terminal kinase, and apoptosis, *Journal of immunology (Baltimore, Md. : 1950)*, 163 (1999) 6800-6809.
- [31] S. Dhanalakshmi, R.P. Singh, C. Agarwal, R. Agarwal, Silibinin inhibits constitutive and TNFalpha-induced activation of NF-kappaB and sensitizes human prostate carcinoma DU145 cells to TNFalpha-induced apoptosis, *Oncogene*, 21 (2002) 1759-1767.
- [32] S.J. Polyak, P. Ferenci, J.M. Pawlotsky, Hepatoprotective and antiviral functions of silymarin components in hepatitis C virus infection, *Hepatology (Baltimore, Md.)*, 57 (2013) 1262-1271.
- [33] V. Kren, J. Ulrichova, P. Kosina, D. Stevenson, P. Sedmera, V. Prikrylova, P. Halada, V. Simanek, Chemoenzymatic preparation of silybin beta-glucuronides and their biological evaluation, *Drug metabolism and disposition: the biological fate of chemicals*, 28 (2000) 1513-1517.
- [34] H. Zhao, G.E. Brandt, L. Galam, R.L. Matts, B.S. Blagg, Identification and initial SAR of silybin: an Hsp90 inhibitor, *Bioorganic & medicinal chemistry letters*, 21 (2011) 2659-2664.
- [35] F. Wang, K. Huang, L. Yang, J. Gong, Q. Tao, H. Li, Y. Zhao, S. Zeng, X. Wu, J. Stockigt, X. Li, J. Qu, Preparation of C-23 esterified silybin derivatives and evaluation of their lipid peroxidation inhibitory and DNA protective properties, *Bioorganic & medicinal chemistry*, 17 (2009) 6380-6389.
- [36] P. Kidd, K. Head, A review of the bioavailability and clinical efficacy of milk thistle phytosome: a silybin-phosphatidylcholine complex (Siliphos), *Alternative medicine review : a journal of clinical therapeutic*, 10 (2005) 193-203.
- [37] R. Gazak, A. Svobodova, J. Psotova, P. Sedmera, V. Prikrylova, D. Walterova, V. Kren, Oxidised derivatives of silybin and their antiradical and antioxidant activity, *Bioorganic & medicinal chemistry*, 12 (2004) 5677-5687.
- [38] F.E. Koehn, G.T. Carter, The evolving role of natural products in drug discovery, *Nature reviews. Drug discovery*, 4 (2005) 206-220.
- [39] A. Rowan, Lead Optimization: Improving natural strength, *Nature reviews. Drug discovery*, 4 (2005) 1041-1041.

- [40] Z. Xiao, S.L. Morris-Natschke, K.H. Lee, Strategies for the optimization of natural leads to anticancer drugs or drug candidates, *Medicinal research reviews*, 36 (2016) 32-91.
- [41] C. Morice, C.G. Wermuth, Chapter 9 - Ring Transformations, in: *The Practice of Medicinal Chemistry (Fourth Edition)*, Academic Press, San Diego, 2008, pp. 243-266.
- [42] Z. Wang, Claisen-Schmidt Condensation, in: *Comprehensive Organic Name Reactions and Reagents*, John Wiley & Sons, Inc., 2010.
- [43] R. Gazak, D. Walterova, V. Kren, Silybin and silymarin-new and emerging applications in medicine, *Current medicinal chemistry*, 14 (2007) 315-338.
- [44] H. Kauntz, S. Bousserouel, F. Gosse, F. Raul, Silibinin triggers apoptotic signaling pathways and autophagic survival response in human colon adenocarcinoma cells and their derived metastatic cells, *Apoptosis : an international journal on programmed cell death*, 16 (2011) 1042-1053.
- [45] M. Kaur, B. Velmurugan, A. Tyagi, C. Agarwal, R.P. Singh, R. Agarwal, Silibinin suppresses growth of human colorectal carcinoma SW480 cells in culture and xenograft through down-regulation of β -catenin-dependent signaling, *Neoplasia*, 12 (2010) 415-424.
- [46] M. Kaur, B. Velmurugan, A. Tyagi, G. Deep, S. Katiyar, C. Agarwal, R. Agarwal, Silibinin suppresses growth and induces apoptotic death of human colorectal carcinoma LoVo cells in culture and tumor xenograft, *Molecular cancer therapeutics*, 8 (2009) 2366-2374.
- [47] C. Lin, J.S. Yang, S.C. Tsai, C.F. Lin, M.R. Lee, In vivo evaluation of the synthesized novel 2-benzyloxybenzaldehyde analog CCY-1a-E2 for the treatment of leukemia in the BALB/c mouse WEHI-3 allograft model, *Oncology letters*, 5 (2013) 777-782.
- [48] C.F. Lin, J.S. Yang, C.Y. Chang, S.C. Kuo, M.R. Lee, L.J. Huang, Synthesis and anticancer activity of benzyloxybenzaldehyde derivatives against HL-60 cells, *Bioorganic & medicinal chemistry*, 13 (2005) 1537-1544.
- [49] R.S. Wong, Apoptosis in cancer: from pathogenesis to treatment, *Journal of Experimental & Clinical Cancer Research*, 30 (2011) 87.
- [50] G. Mariño, G. Kroemer, Mechanisms of apoptotic phosphatidylserine exposure, *Cell Research*, 23 (2013) 1247-1248.
- [51] I. Vermes, C. Haanen, H. Steffens-Nakken, C. Reutellingsperger, A novel assay for apoptosis Flow cytometric detection of phosphatidylserine expression on early apoptotic cells using fluorescein labelled Annexin V, *Journal of Immunological Methods*, 184 (1995) 39-51.
- [52] G. Steinberg, U. Fuchs, The role of microtubules in cellular organization and endocytosis in the plant pathogen *Ustilago maydis*, *Journal of microscopy*, 214 (2004) 114-123.

- [53] P. Kosina, P. Maurel, J. Ulrichova, Z. Dvorak, Effect of silybin and its glycosides on the expression of cytochromes P450 1A2 and 3A4 in primary cultures of human hepatocytes, *Journal of biochemical and molecular toxicology*, 19 (2005) 149-153.
- [54] B.A. Lodish H, Zipursky SL, et al, *Microtubule Dynamics and Motor Proteins during Mitosis*, in: *Molecular Cell Biology*, W. H. Freeman, New York, 2000.
- [55] Y. Lu, J. Chen, M. Xiao, W. Li, D.D. Miller, An Overview of Tubulin Inhibitors That Interact with the Colchicine Binding Site, *Pharmaceutical research*, 29 (2012) 2943-2971.
- [56] S. Ducki, Antimitotic chalcones and related compounds as inhibitors of tubulin assembly, *Anti-Cancer Agents in Medicinal Chemistry (Formerly Current Medicinal Chemistry-Anti-Cancer Agents)*, 9 (2009) 336-347.
- [57] R.B.G. Ravelli, B. Gigant, P.A. Curmi, I. Jourdain, S. Lachkar, A. Sobel, M. Knossow, Insight into tubulin regulation from a complex with colchicine and a stathmin-like domain, *Nature*, 428 (2004) 198-202.
- [58] R.A. Friesner, J.L. Banks, R.B. Murphy, T.A. Halgren, J.J. Klicic, D.T. Mainz, M.P. Repasky, E.H. Knoll, M. Shelley, J.K. Perry, D.E. Shaw, P. Francis, P.S. Shenkin, Glide: A New Approach for Rapid, Accurate Docking and Scoring. 1. Method and Assessment of Docking Accuracy, *Journal of Medicinal Chemistry*, 47 (2004) 1739-1749.
- [59] S. Ducki, G. Mackenzie, B. Greedy, S. Armitage, J.F.D. Chabert, E. Bennett, J. Nettles, J.P. Snyder, N.J. Lawrence, Combretastatin-like chalcones as inhibitors of microtubule polymerisation. Part 2: Structure-based discovery of alpha-aryl chalcones, *Bioorganic & Medicinal Chemistry*, 17 (2009) 7711-7722.
- [60] W.L. Jorgensen, J. Tirado-Rives, The OPLS [optimized potentials for liquid simulations] potential functions for proteins, energy minimizations for crystals of cyclic peptides and crambin, *Journal of the American Chemical Society*, 110 (1988) 1657-1666.

Highlights:

- Synthesis of novel silybin derivatives by ring disjunctive natural lead optimization
- **15k** discovered to be highly potent and selective to ovarian cancer cells
- **15k** induces sub-G1 cell cycle arrest and induces apoptosis
- **15k** binds with high affinity to tubulin and inhibits their expression

ACCEPTED MANUSCRIPT